

ARTICLE

TLR8 and its endogenous ligand miR-21 contribute to neuropathic pain in murine DRG

Zhi-Jun Zhang^{1,2*}, Jian-Shuang Guo^{1*}, Si-Si Li^{1*}, Xiao-Bo Wu¹, De-Li Cao¹, Bao-Chun Jiang¹, Peng-Bo Jing¹, Xue-Qiang Bai², Chun-Hua Li¹, Zi-Han Wu^{1,2}, Ying Lu^{1,3}, and Yong-Jing Gao^{1,4} 

Toll-like receptors (TLRs) are nucleic acid-sensing receptors and have been implicated in mediating pain and itch. Here we report that *Tlr8*^{-/-} mice show normal itch behaviors, but have defects in neuropathic pain induced by spinal nerve ligation (SNL) in mice. SNL increased TLR8 expression in small-diameter IB4⁺ DRG neurons. Inhibition of TLR8 in the DRG attenuated SNL-induced pain hypersensitivity. Conversely, intrathecal or intradermal injection of TLR8 agonist, VTX-2337, induced TLR8-dependent pain hypersensitivity. Mechanistically, TLR8, localizing in the endosomes and lysosomes, mediated ERK activation, inflammatory mediators' production, and neuronal hyperexcitability after SNL. Notably, miR-21 was increased in DRG neurons after SNL. Intrathecal injection of miR-21 showed the similar effects as VTX-2337 and inhibition of miR-21 in the DRG attenuated neuropathic pain. The present study reveals a previously unknown role of TLR8 in the maintenance of neuropathic pain, suggesting that miR-21-TLR8 signaling may be potential new targets for drug development against this type of chronic pain.

Introduction

TLRs are a family of transmembrane pattern recognition receptors which mediate innate and adaptive immunity by recognizing exogenous ligands, pathogen-associated molecular patterns, and danger-associated molecular patterns (Akira et al., 2006). Currently, 10 functional TLRs in humans (TLR1–TLR10) and 12 in mice (TLR1–TLR9 and TLR11–TLR13) have been reported. TLRs 1, 2, 4, 5, 6, and 10 are located in the plasma membrane to recognize bacterial membrane components, whereas TLRs 3, 7, 8, and 9 are predominantly located within intracellular compartments to recognize nucleic acid-based ligands (Kawai and Akira, 2010). TLRs are not only expressed in immune system, but also expressed in neurons and nonneuronal cells (such as astrocytes and microglia) of the nervous system (Kielian, 2006; Crack and Bray, 2007). Recent studies have demonstrated that several TLRs play pivotal roles in the pathogenesis of pain and itch in the dorsal root ganglion (DRG) and spinal cord (Liu et al., 2012b). For example, TLR2 and TLR4 modulate glial activation in the spinal cord and contribute to the development of neuropathic pain (Tanga et al., 2005; Li et al., 2015). Spinal TLR4 is also involved in chronic itch via mediating astrocyte activation (Liu et al., 2016). TLR3, which is expressed by small-diameter TRPV1-positive DRG neurons, is vital in regulating sensory neuronal excitability, spinal synaptic transmission and central sensitization (Liu et al., 2012a).

The intracellular TLRs, including TLR3, TLR7, TLR8, and TLR9, detect nucleic acid-based ligands: TLR3 senses viral double-stranded RNA (dsRNA; Alexopoulou et al., 2001), and TLR7 and TLR8 recognize viral single-stranded RNA (ssRNA; Diebold et al., 2004; Heil et al., 2004), while TLR9 detects bacterial and viral unmethylated CpG-containing DNA motifs (Hemmi et al., 2000). Among these TLRs, *Tlr7* and *Tlr8* genes show high homology to each other and are both located on the X chromosome (Kawai and Akira, 2010). In the past decade, TLR8 has been less investigated than TLR7, as TLR8 was considered previously to be nonfunctional in mice (Jurk et al., 2002). However, recent studies have shown that TLR8 is a negative regulator of neurite outgrowth and an inducer of neuronal apoptosis in mice (Ma et al., 2006, 2007). TLR8 expression is also up-regulated in mouse central nervous system (CNS) in response to the microbial challenge (Olson and Miller, 2004) and during the progression of experimental autoimmune encephalomyelitis (Prinz et al., 2006). These data suggest that TLR8 is not only active, but also has a distinct biological function. Recently, TLR7 was shown to be expressed in DRG neurons and was involved in itch via coupling with TRPA1 in the DRG (Liu et al., 2010). It is interesting to investigate whether TLR8 is involved in itch/pain and the implicated mechanisms.

¹Pain Research Laboratory, Institute of Nautical Medicine, Nantong University, Jiangsu, China; ²Department of Human Anatomy, School of Medicine, Nantong University, Jiangsu, China; ³Department of Nutrition and Food Hygiene, School of Public Health, Nantong University, Jiangsu, China; ⁴Co-innovation Center of Neuroregeneration, Nantong University, Jiangsu, China.

*Z.-J. Zhang, J.-S. Guo, and S.-S. Li contributed equally to this work; Correspondence to Yong-Jing Gao: gaoyongjing@hotmail.com or gaoyongjing@ntu.edu.cn.

© 2018 Zhang et al. This article is distributed under the terms of an Attribution–Noncommercial–Share Alike–No Mirror Sites license for the first six months after the publication date (see <http://www.rupress.org/terms/>). After six months it is available under a Creative Commons License (Attribution–Noncommercial–Share Alike 4.0 International license, as described at <https://creativecommons.org/licenses/by-nc-sa/4.0/>).

Most TLRs signal through a conserved canonical pathway initiated by the association of the adaptor protein myeloid differentiation primary response protein 88 (MyD88) with TLR intracellular domains. MyD88 recruits the IL-1 receptor (IL-1R)-associated kinases, which leads to the activation of NF κ B and further initiates the transcription of numerous proinflammatory mediators (Liu et al., 2012b). Also, TLR8 recognizes ssRNA and endogenous RNAs, such as microRNAs, and leads to the production of proinflammatory cytokines (Fabbri et al., 2012; Sarvestani et al., 2012). A recent study showed that tumor-secreted microRNA (miR)-21 and miR-29a bind to TLR8 in human immune cells, triggering a TLR-mediated prometastatic inflammatory response that ultimately leads to tumor growth and metastasis (Fabbri et al., 2012). Whether endogenous microRNAs can activate TLR8 in the DRG and lead intracellular kinase-mediated inflammatory mediator production after nerve injury remains unknown.

In the present study, we investigated the role of TLR8 in the DRG in itch and pain using *Tlr8*^{-/-} mice. We found that TLR8 plays a different role from TLR7, as it is not involved in itch, but is involved in neuropathic pain. Besides, TLR8 is expressed in intracellular organelles of small- and medium-sized neurons in the DRG. Mechanistically, TLR8 is activated by miR-21 and leads to ERK-mediated (but not NF κ B-mediated) production of inflammatory mediators and neuronal hyperexcitability during neuropathic pain.

Results

Generation and characterization of *Tlr8*^{-/-} mice

To determine the role of TLR8 in itch and pain, *Tlr8*^{-/-} mice were generated (Fig. S1 A). The deletion of 12 bases on Exon 2 of *Tlr8* was confirmed by DNA sequencing (Fig. S1 B) and PCR (Fig. S1 C). TLR8 immunostaining showed signals in the DRG of WT mice, but not in *Tlr8*^{-/-} mice (Fig. S1 D). Also, *Tlr8*^{-/-} mice had normal growth (Fig. S1 E) and normal size of body, spleen, thymus, and LN (Fig. S1 F and G), and did not develop symptoms of illness (such as diarrhea). TLR7 expression in the spleen, DRG, and spinal cord of *Tlr8*^{-/-} mice was comparable to that of WT littermates (Fig. S1, H and I). Furthermore, *Tlr8*^{-/-} mice had normal expression pattern of the neurons (Nissl staining) and normal innervations of the primary afferents, labeled with calcitonin gene-related peptide (CGRP) and isolectin B4 (IB4) in the spinal cord dorsal horn (Fig. S2 A). In the DRG, the distribution and the number of neurons (Nissl staining) are comparable between *Tlr8*^{-/-} mice and WT littermates. The expression of CGRP, IB4, and NF200 in *Tlr8*^{-/-} mice is also indistinguishable from WT mice (Fig. S2 B). The distribution of nerve fibers, labeled with PGP9.5 in the skin of paw and nape of *Tlr8*^{-/-} mice, was not different from that of WT mice (Fig. S2 C). These data suggest that *Tlr8*^{-/-} mice do not have developmental and immunological defects, and the deletion of *Tlr8* did not affect the expression of TLR7.

Tlr8^{-/-} mice show normal itch and pain responses but impaired chronic pain

We then performed behavioral tests in *Tlr8*^{-/-} mice and WT littermates. First, intradermal injection of histamine-dependent agents (histamine and compound 48/80), histamine-in-

dependent agent (chloroquine; CQ), TLR7 agonists (imiquimod and loxoribine), or TLR7/8 agonist (R848) induced comparable scratches in *Tlr8*^{-/-} and WT littermates (Fig. S3, A–F). Second, *Tlr8*^{-/-} mice were indistinguishable from WT littermates with respect to nociceptive behaviors elicited by noxious heat (tail flick test and Hargreaves test; Fig. S3, G and H) and von Frey mechanical stimulation (Fig. S3 I). In addition, the rotarod test revealed similar falling latency in WT and *Tlr8*^{-/-} mice (Fig. S3 J). Third, peripheral injection of formalin induced two-phase spontaneous pain in WT and *Tlr8*^{-/-} mice (Fig. S3 K). Intradermal injection of capsaicin also induced similar licking and flinching behaviors in WT and *Tlr8*^{-/-} mice (Fig. S3 L). These data suggest that *Tlr8* deletion did not affect acute itch, normal pain sensation, motor function, and acute inflammatory pain.

We further tested chronic neuropathic pain and inflammatory pain. Nerve injury induced persistent mechanical allodynia, which started from day 3 and was maintained for >21 d in WT mice. However, the mechanical allodynia was considerably alleviated in *Tlr8*^{-/-} mice from 10 d after spinal nerve ligation (SNL; Fig. 1 A). Heat hyperalgesia was alleviated in *Tlr8*^{-/-} mice from 7 d after SNL (Fig. 1 B). Intraperitoneal injection of paclitaxel (PTX)-induced mechanical allodynia was also significantly reduced in *Tlr8*^{-/-} mice (Fig. 1 C). In contrast, intraplantar injection of CFA-induced mechanical allodynia was only mildly reduced at day 3 in *Tlr8*^{-/-} mice (Fig. 1 D). These data suggest that TLR8 play an essential role in the maintenance of neuropathic pain.

As glial cells (astrocytes and microglia) are activated in the spinal cord after nerve injury, and glial activation is correlated with the neuropathic pain (Gao and Ji, 2010), we further examined the expression of astrocytic marker GFAP and microglial marker IBA-1 in the spinal cord 10 d after sham operation or SNL. Quantitative real-time PCR showed that the mRNA expression of GFAP and IBA1 was increased in WT mice, but was reduced in *Tlr8*^{-/-} mice (Fig. 1, E and F). The immunostaining also showed the reduced intensity of GFAP and IBA-1 signal in *Tlr8*^{-/-} mice, compared with WT mice (Fig. 1, G–P), supporting the pivotal role of TLR8 in the pathogenesis of neuropathic pain.

TLR8 is increased in the spinal cord after SNL

The spinal cord is important in mediating pain transmission and modulation. We first checked the expression and distribution of TLR8 in the spinal cord. In naive mice, TLR8 had low expression in the superficial dorsal horn and ventral horn (Fig. 2 A). In contrast, TLR8-IR was dramatically increased in the ipsilateral dorsal horn and ventral horn, with no apparent change in the contralateral side 10 d after SNL (Fig. 2, B–E). Additionally, TLR8 was mainly expressed in fibers in the dorsal horn (Fig. 2 C). Double staining showed that TLR8 was not colocalized with neuronal marker NeuN (Fig. 2 F), astrocytic marker GFAP (Fig. 2 G), or microglial marker OX-42 (Fig. 2 H) in the dorsal horn 10 d after SNL. To identify the source of TLR8, L5 dorsal root ligation was performed after SNL. 10 d after the operation, TLR8 protein was accumulated at the ligation part proximal to the DRG (Fig. 2 I). Meanwhile, TLR8 was not increased in the ipsilateral dorsal horn (Fig. 2, J–L), but was still increased in neurons of the ipsilateral ventral horn (Fig. 2 J), suggesting that TLR8 in the dorsal horn is transported from the DRG neurons.

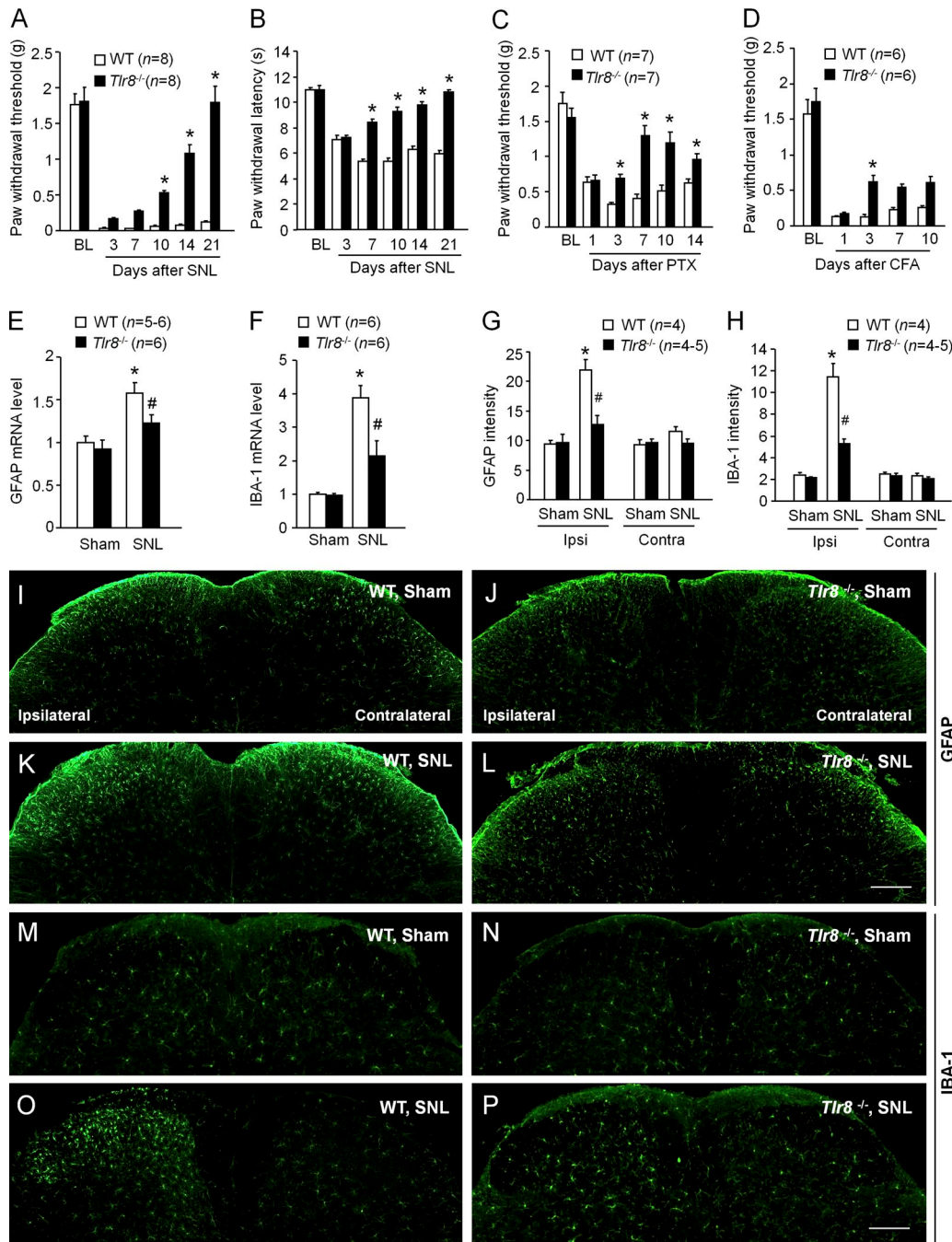


Figure 1. *Tlr8* deletion alleviates neuropathic pain and glial activation induced by SNL. **(A and B)** The mechanical allodynia (A) and heat hyperalgesia (B) were attenuated in *Tlr8^{-/-}* mice following SNL. $n = 8$ mice per group. **(C)** Intraperitoneal injection of PTX (6 mg/kg)-induced mechanical allodynia was markedly alleviated in *Tlr8^{-/-}* mice. $n = 7$ mice per group. **(D)** Intraplantar injection of CFA (20 μ l)-induced mechanical allodynia was mildly attenuated at Day 3 in *Tlr8^{-/-}* mice. $n = 6$ mice per group. *, $P < 0.05$ compared with WT. Two-way RM ANOVA followed by post hoc Bonferroni's test. Data are representative of two independent experiments. **(E and F)** The quantitative PCR analysis shows that the expression of GFAP (E) and IBA-1 (F) mRNA was reduced in *Tlr8^{-/-}* mice. $n = 5-6$ mice per group. *, $P < 0.05$ compared with WT-sham. #, $P < 0.05$ compared with WT-SNL. Two-way ANOVA followed by post hoc Bonferroni's test. **(G and H)** Immunofluorescence intensity analysis shows that the immunoreactivity of GFAP (G) and IBA-1 (H) in the spinal dorsal horn was reduced in *Tlr8^{-/-}* mice. $n = 4-5$ mice per group. *, $P < 0.05$ compared with WT-sham. #, $P < 0.05$ compared with WT-SNL. Two-way ANOVA followed by post hoc Bonferroni's test. **(I-L)** The immunofluorescence staining of GFAP in the spinal dorsal horn in WT and *Tlr8^{-/-}* mice at SNL or sham 10 d. Bar, 200 μ m. **(M-P)** The immunofluorescence staining of IBA-1 in the spinal dorsal horn in WT and *Tlr8^{-/-}* mice at SNL or sham 10 d. Bar, 200 μ m. All data are means \pm SEM.

TLR8 is mainly expressed in small DRG neurons and is increased after SNL

We then examined TLR8 expression in the DRG after SNL. SNL increased TLR8 mRNA expression at days 3, 10, and 21 in the in-

jured L5 DRGs (Fig. 3 A). Immunostaining showed that TLR8 is mainly expressed in small- ($<300 \mu$ m; 54.9%) and medium-sized (300–600 μ m; 38.1%) DRG neurons in naive mice (Fig. 3 B). After SNL, both the percentage of TLR8⁺ neurons and the intensity of

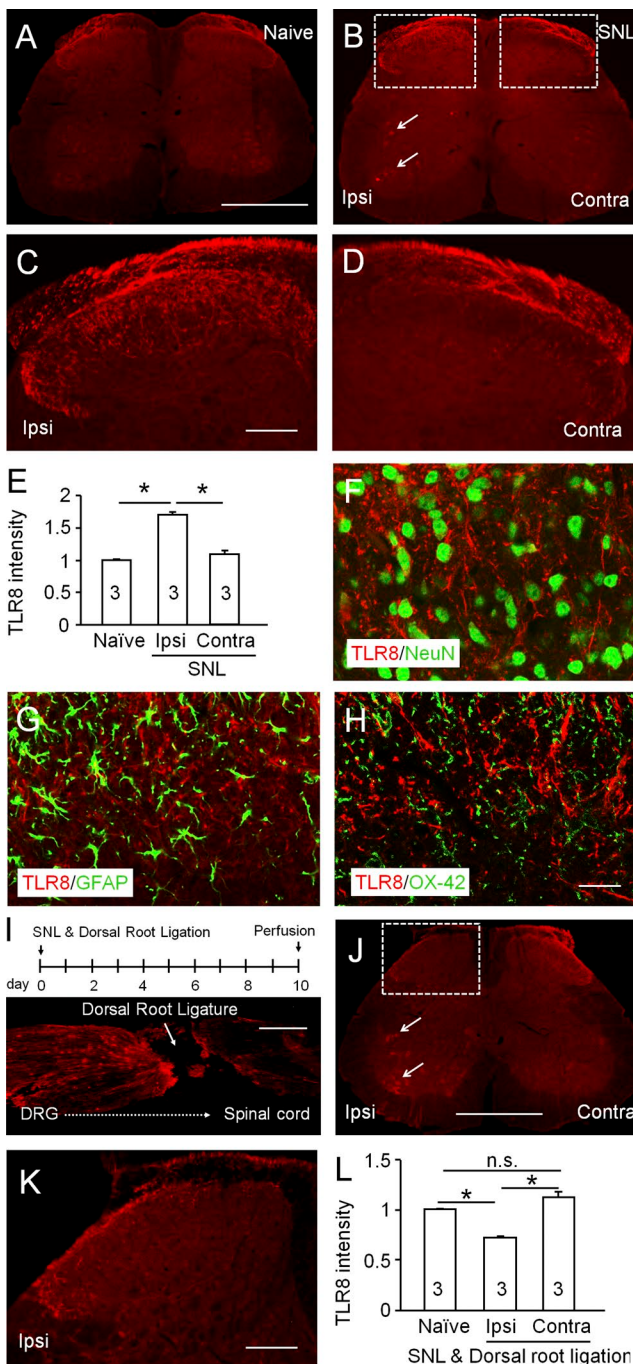


Figure 2. The expression and distribution of TLR8 in the spinal cord after SNL. (A and B) The TLR8 immunofluorescence staining in the spinal cord of naïve (A) and SNL 10 d (B) mice. The arrows in B show the TLR8⁺ neurons in the spinal ventral horn. Ipsi, ipsilateral. Contra, contralateral. Bar, 500 µm. **(C and D)** The higher magnification images in the boxes of B. Bar, 100 µm. **(E)** Statistical analysis shows the TLR8 intensity in the dorsal horn of naïve mice and in the ipsilateral (Ipsi) and contralateral (Contra) side of SNL mice (10 d). *, P < 0.05, one-way ANOVA followed by Bonferroni's test. Data are representative of two independent experiments. **(F–H)** Representative images of double staining of TLR8 with NeuN (F), GFAP (G), and OX-42 (H). Bar, 20 µm. **(I)** The TLR8 immunostaining in the dorsal root. Top, schematic illustrating the timeline of the operation and staining. Bottom, the distribution of TLR8 in the ligated dorsal root. Note that the dorsal root ligation following SNL resulted in TLR8 accumulation in the distal site of ligation. Bar, 200 µm. **(J)** The TLR8 immunofluorescence staining in the spinal cord 10 d after SNL with dorsal root ligation. Note that the TLR8-IR was not increased in the ipsilateral dorsal

horn but was still increased in the ipsilateral ventral horn. The arrows show the TLR8⁺ neurons in the spinal ventral horn. Bar, 500 µm. **(K)** The higher magnification images in the box of J. Bar, 100 µm. **(L)** Statistical analysis shows the TLR8 intensity in the dorsal horn of naïve mice and in the ipsilateral side and contralateral side of mice with SNL and dorsal root ligation. *, P < 0.05. One-way ANOVA followed by post hoc Bonferroni's test. n.s., not significant. Data are representative of two independent experiments.

TLR8-IR were increased at days 3, 10, and 21 in small and medium neurons (Fig. 3, C–I). Further double staining of TLR8 with neuronal marker TuJ1 showed that TLR8 was wholly colocalized with TuJ1 in naïve mice (Fig. 3 J). 10 d after SNL, TLR8 was still colocalized with TuJ1 (Fig. 3 K) and not with satellite cell marker GFAP (Fig. 3 L) or macrophage marker CD68 (Fig. 3 M).

To examine the expression and distribution of TLR8 in human DRG, we did a staining of TLR8, peripherin, and Nissl in L5 DRG sections (Fig. S4, A–G). TLR8 was expressed in 55.2% DRG neurons, and 57.4% of TLR8⁺ neurons expressed small-diameter neuronal marker peripherin (Fig. S4, H and I), suggesting similar distribution pattern of TLR8 in the DRG of mice and human.

TLR8 is mainly expressed in IB4⁺ neurons and is partially colocalized with TLR

Next, we characterize the neurochemistry of TLR8 positive cells in the DRG. TLR8 was double-stained with nonpeptidergic marker IB4 (Fig. 3 N), peptidergic marker CGRP (Fig. 3 O), and large neuronal marker neurofilament 200 (NF200; Fig. 3 P). It showed that 85.5% of IB4⁺ neurons expressed TLR8, while 64.1% of TLR8-expressing neurons were IB4⁺. Of CGRP⁺ DRG neurons, 36.3% expressed TLR8 and 23.2% of TLR8⁺ neurons exhibited CGRP binding. Of NF200⁺ neurons, 5.0% expressed TLR8 and 3.5% of TLR8⁺ neurons expressed NF200 (Fig. 3 Q). Single-cell RT-PCR showed that 8 of 12 (66.7%) IB4⁺ neurons and 2 of 11 (18.2%) IB4⁻ neurons expressed TLR8 (Fig. 3 R and S). These findings indicate that TLR8 is mainly expressed in IB4⁺ neurons.

As TLR7 is highly homologous to TLR8 (Chuang and Ulevitch, 2000), we then characterized the expression of TLR7 in the DRG. Double staining of TLR7 with IB4, CGRP, and NF200 showed that TLR7 was expressed in both IB4⁺ and CGRP⁺ neurons, with a few in NF200⁺ neurons (Fig. 3, T–V). Further single-cell RT-PCR showed that 5 of 10 (50%) IB4⁺ neurons and 2 of 10 (20%) IB4⁻ neurons expressed TLR7. Among these TLR7⁺ cells, 4 of 7 also expressed TLR8, and 4 of 10 TLR8⁺ cells expressed TLR7 (Fig. 3 W), suggesting that TLR7 and TLR8 are partially coexpressed in DRG neurons.

TLR8 in the DRG is necessary for the maintenance of neuropathic pain

To check whether TLR8 in the DRG is involved in neuropathic pain, we delivered TLR8-targeting siRNA to the L5 spinal nerve of C57BL/6 mice. To enable siRNA binding to neurons and enhance knockdown efficiency, the siRNA was mixed with a short peptide derived from the rabies virus glycoprotein (RVG-9R; Berta et al., 2014). Peri-spinal nerve delivery of TLR8 siRNA (2 µg) effectively attenuated SNL-induced mechanical allodynia (Fig. 4 A) and heat hyperalgesia (Fig. 4 B) from 3 d after SNL. The siRNA treatment

horn but was still increased in the ipsilateral ventral horn. The arrows show the TLR8⁺ neurons in the spinal ventral horn. Bar, 500 µm. **(K)** The higher magnification images in the box of J. Bar, 100 µm. **(L)** Statistical analysis shows the TLR8 intensity in the dorsal horn of naïve mice and in the ipsilateral side and contralateral side of mice with SNL and dorsal root ligation. *, P < 0.05. One-way ANOVA followed by post hoc Bonferroni's test. n.s., not significant. Data are representative of two independent experiments.

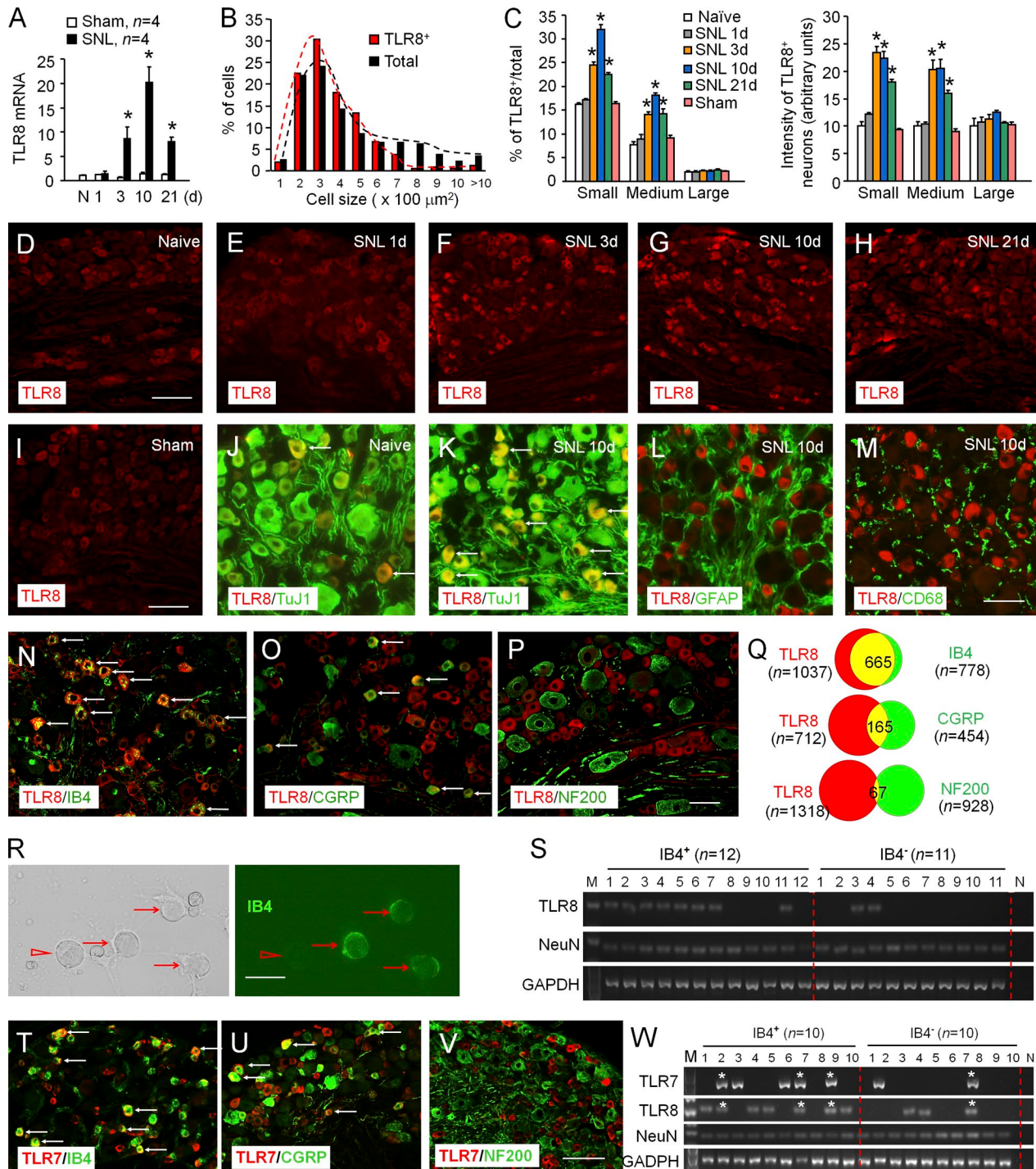


Figure 3. The expression and distribution of TLR8 in the DRG after SNL. **(A)** The time-course of TLR8 mRNA expression in L5 DRG after SNL and sham operation. $n = 4$ mice per group. *, $P < 0.05$ compared with the corresponding sham group. Two-way ANOVA followed by post hoc Bonferroni's test. Data are representative of two independent experiments. **(B)** The cell-size distribution frequency of TLR8⁺ neurons and total neurons in the DRG of naive mice. **(C)** The percentage of TLR8⁺ neurons (left panel) and intensity of TLR8-IR (right panel) in the small-, medium-, and large-sized DRG neurons in naive, sham, and SNL mice. $n = 3$ mice per group. *, $P < 0.05$ compared with the corresponding sham group. Student's unpaired t test. **(D–H)** The representative images of TLR8 staining in the DRG of naive, sham, and SNL mice. Bar, 100 μ m. **(I–M)** The double staining of TLR8 with TuJ1 (J and K), GFAP (L), and CD68 (M). The arrows indicate the typical double-labeled neurons. Bar, 50 μ m. **(N–P)** The double immunostaining of TLR8/IB4 (N), TLR8/CGRP (O), and TLR8/NF200 (P) in naive DRG sections. The arrows indicate the double-labeled neurons. Bar, 50 μ m. **(Q)** The Venn diagrams showing the double staining of TLR8⁺ with the IB4⁺, CGRP⁺, and NF200⁺. **(R)** The images of cultured DRG neurons incubated with IB4. Left, bright field. Right, fluorescence image. Arrow, IB4⁺ neurons. Triangle, IB4⁻ neurons. Bar, 25 μ m. **(S)** Single-cell RT-PCR analysis from IB4⁺ and IB4⁻ neurons showing the expression of TLR8 mRNA. N, negative control. Numbers on the top of gels indicate individual DRG neurons. Data are representative of two independent experiments. **(T–V)** The double immunostaining of TLR7/IB4 (T), TLR7/CGRP (U), and TLR7/NF200 (V) in naive DRG sections. The arrows indicate the double-labeled neurons. Bar, 100 μ m. **(W)** Single-cell RT-PCR analysis of the cultured DRG neurons showing the coexpression of TLR7 with TLR8, NeuN, and GAPDH. Asterisk indicates coexpression of *Tlr7* and *Tlr8* in a single neuron. Data are representative of two independent experiments.

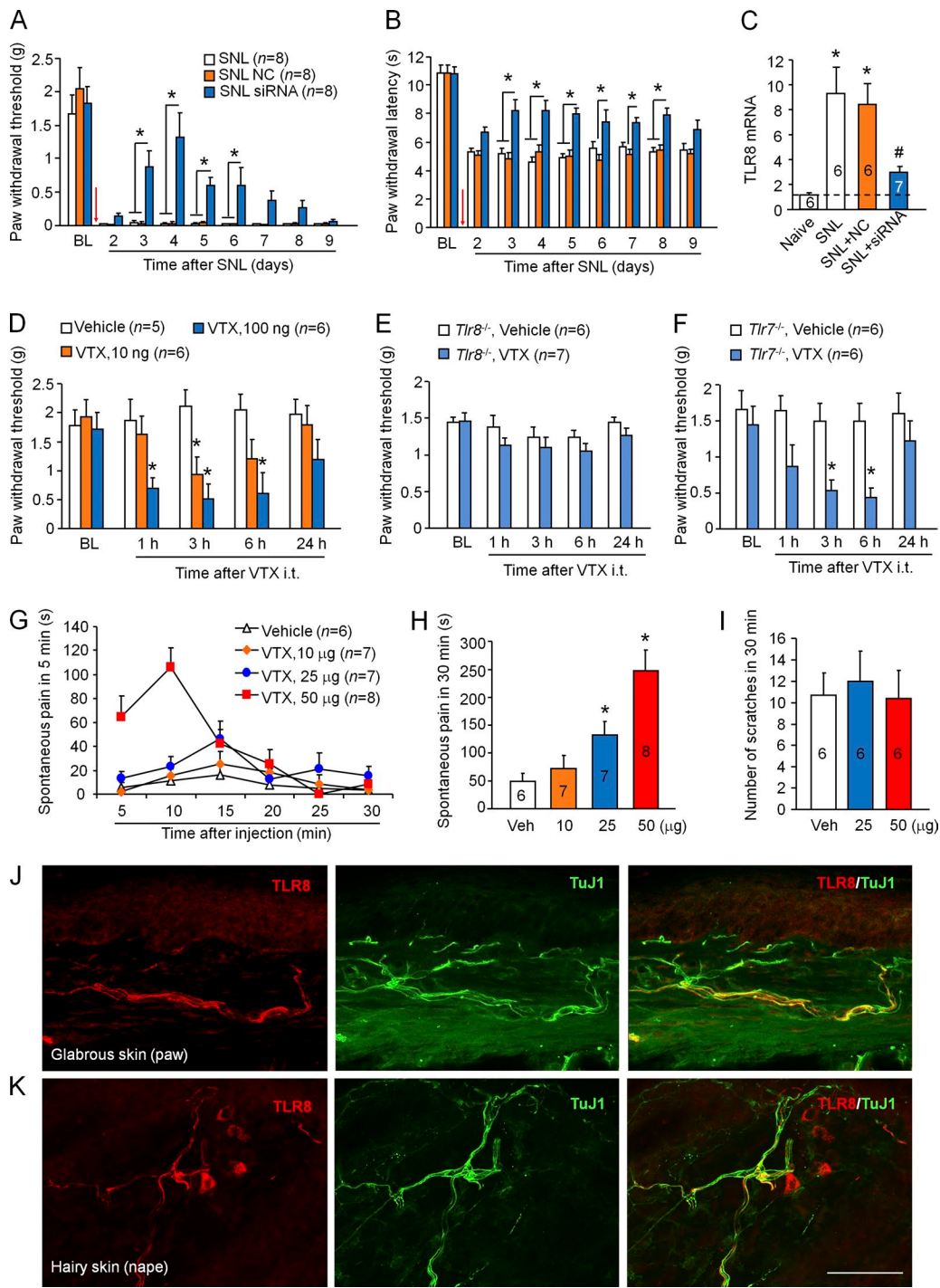


Figure 4. The knockdown or activation of TLR8 affects the pain behaviors. (A and B) Peri-spinal nerve delivery of TLR8 siRNA (2 µg mixed with the RVG peptide) alleviated the mechanical allodynia (A) and heat hyperalgesia (B) induced by SNL. $n = 8$ mice per group. NC, negative control siRNA. *, $P < 0.05$ compared with SNL only or SNL+NC group. Two-way RM ANOVA followed by post hoc Bonferroni's test. Data are representative of two independent experiments. (C) Quantitative PCR of DRG tissues shows that TLR8 siRNA down-regulated TLR8 mRNA expression. $n = 6\text{--}7$ mice per group. *, $P < 0.05$ compared with the naive group. #, $P < 0.05$ compared with SNL + NC group. One-way ANOVA followed by post hoc Bonferroni's test. Data are representative of two independent experiments. (D) Intrathecal injection of VTX (VTX-2337) dose-dependently decreased the paw withdrawal threshold in WT mice. $n = 5\text{--}6$ mice per group. *, $P < 0.05$ compared with vehicle (PBS) group. Two-way RM ANOVA followed by post hoc Bonferroni's test. Data are representative of two independent experiments. (E) Intrathecal injection of VTX did not affect the paw withdrawal threshold in *Tlr8^{-/-}* mice. $n = 6\text{--}7$ mice per group. $P > 0.05$. Two-way RM ANOVA followed by post hoc Bonferroni's test. Data are representative of three independent experiments. (F) Intrathecal injection of VTX induced a decrease of the paw withdrawal threshold in *Tlr7^{-/-}* mice. $n = 6$ mice per group. *, $P < 0.05$ compared with vehicle group. Two-way RM ANOVA followed by post hoc Bonferroni's test. Data are representative of three independent experiments. (G) The time-course of spontaneous pain in every 5 min after intraplantar injection of VTX. $n = 6\text{--}8$ mice per group. Data are representative of two independent experiments. (H) Histogram shows the summary of spontaneous pain behavior in 30 min following intraplantar injection of VTX. *, $P < 0.05$ compared with vehicle (PBS) group. One-way ANOVA followed by post hoc Bonferroni's test. Veh, vehicle. (I)

also reduced TLR8 mRNA expression in the DRG (Fig. 4 C). These results support a pivotal role of DRG TLR8 in the maintenance of neuropathic pain.

TLR8 agonist is sufficient to induce pain hypersensitivity

We then asked if activation of TLR8 is sufficient to induce pain. VTX-2337 (abbreviated as VTX) is a selective and potent TLR8 agonist (Liu et al., 2012). Intrathecal injection with VTX dose-dependently induced mechanical allodynia (Fig. 4 D), but not heat hyperalgesia (data not shown), in WT mice. VTX at the dose of 100 ng did not induce mechanical allodynia in *Tlr8*^{-/-} mice (Fig. 4 E), but still induced mechanical allodynia in *Tlr7*^{-/-} mice (Fig. 4 F). These data suggest that VTX-induced pain hypersensitivity is dependent on TLR8, but not TLR7.

Next, VTX was intradermally injected into the hind paw of C57BL/6 mice, and spontaneous pain behaviors were counted every 5 min for 30 min. The high dose of VTX (50 µg) induced lifting, flinching, and licking behaviors in the first 15 min (Fig. 4 G and H). To test if VTX can induce itch, it was intradermally injected into the nape. VTX (20 or 50 µg) did not induce scratching behaviors (Fig. 4 I). Immunostaining further showed that TLR8 was expressed in the nerves of both glabrous skin (paw; Fig. 4 J) and hairy skin (nape; Fig. 4 K), supporting the role of TLR8 in pain but not in itch processing.

TLR8 localizes to the early endosomes, lysosomes, and ERs in the DRG neurons

To further investigate the mechanism of TLR8 in neuropathic pain, we analyzed the subcellular localization of TLR8 in the DRG neurons of C57BL/6 mice. High magnification confocal images showed that TLR8 is distributed as punctuate structures in the cytoplasm (Fig. 5 A). Double staining showed that TLR8 was partially colocalized with early endosome antigen 1 (EEA1; Fig. 5, B and C), the lysosome marker (LAMP1; Fig. 5, D and E), and ER marker calnexin (Fig. 5, F and G), with more colocalization with LAMP1 than with EEA1 and calnexin. In addition, SNL increased the expression of TLR8 in endosome, lysosome, and ER (Fig. 5, C, E, and G). These data indicate that TLR8 may exit the ER and is targeted to the endosomes and lysosomes to exert further functions.

TLR8 agonist induces ERK activation and inflammatory mediators' expression in the DRG

As most TLRs signal through the adaptor protein MyD88, leading to the activation (or phosphorylation) of NFκB and further inducing the production of inflammatory mediators (Liu et al., 2012b), we checked the expression of phospho-NFκB (pNFκB) in the DRG after intrathecal injection of VTX (100 ng). However, VTX did not change the expression of pNFκB (Fig. 6 A). We then examined the activation of MAPKs, including p38, JNK, and ERK, which are critical intracellular kinases that mediate chronic pain processing (Ji et al., 2009). The expression of pJNK and pp38 was not sig-

nificantly changed after VTX injection (data not shown), whereas pERK expression was markedly increased after VTX (Fig. 6 A). In addition, VTX treatment did not induce ERK activation in *Tlr8*^{-/-} mice, but still induced ERK activation in *Tlr7*^{-/-} mice (Fig. 6 B). Furthermore, in HEK393 cells transfected with TLR8 plasmid (Fig. 6 C), VTX did not change the luciferase activity at the doses of 0.1, 0.5, and 5 µM in NFκB luciferase reporter assay. However, VTX at the doses of 0.1 and 0.5 µM increased the luciferase activity in ERK assay (Fig. 6 D). These results suggest that VTX induces TLR8-dependent ERK but not NFκB activation in the DRG.

To examine whether VTX-induced pain hypersensitivity and ERK activation are dependent on MyD88, we intrathecally injected VTX in *MyD88*^{-/-} mice. Behavioral tests showed that VTX induced mechanical allodynia in *MyD88*^{-/-} mice, the same as in WT mice (Fig. 6 E). VTX also induced similar ERK activation in WT and *MyD88*^{-/-} mice (Fig. 6 F), indicating that VTX-induced pain hypersensitivity, and ERK activation is not dependent on MyD88.

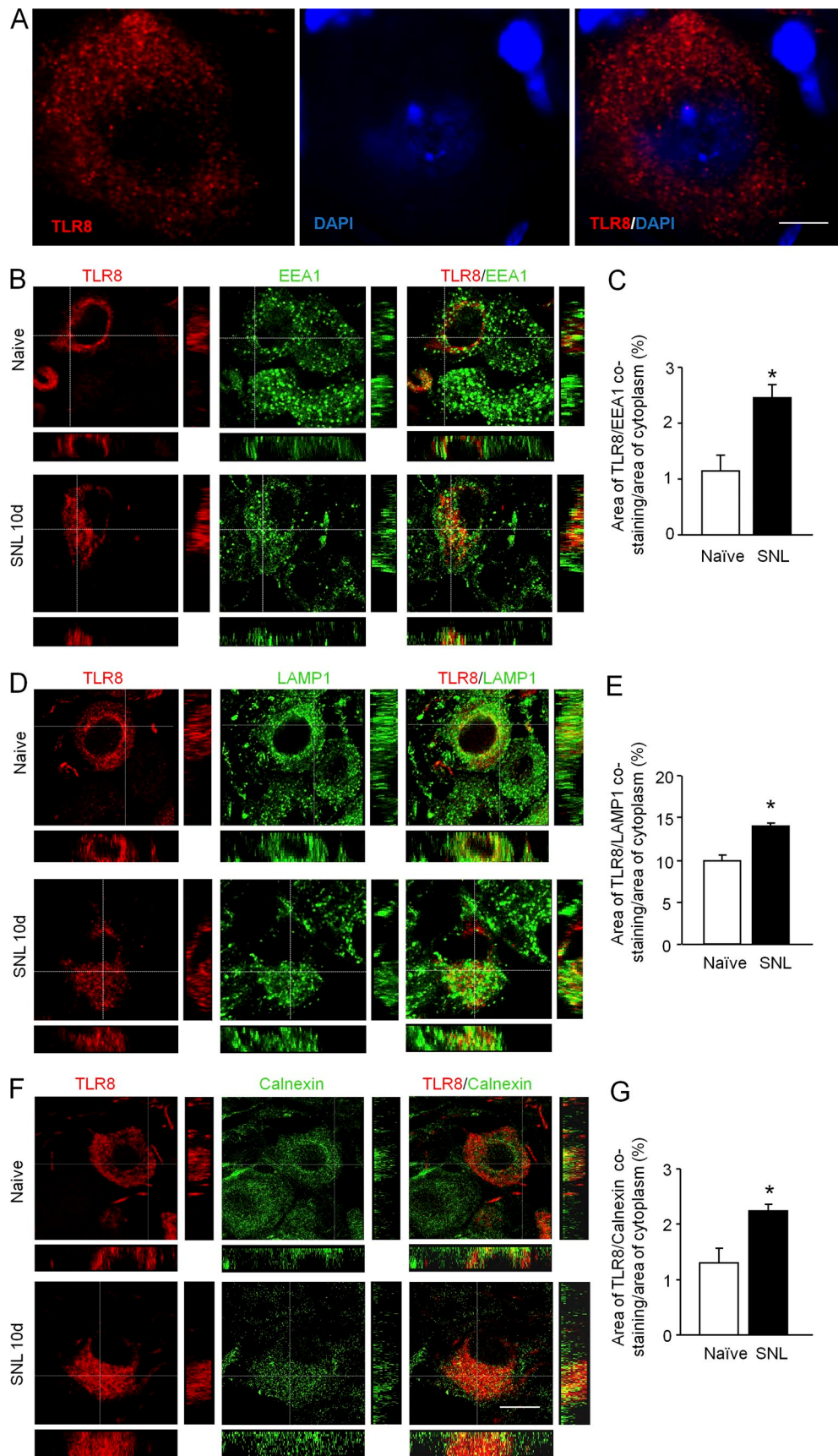
We then examined the inflammatory mediators' expression in the DRG after VTX injection. Proinflammatory cytokines, such as TNF-α, IL-1β, and IL-6, and chemokines, such as CCL2 and CXCL1, are pivotal mediators in driving chronic pain (Kawasaki et al., 2008; Gao et al., 2009; Zhang et al., 2013; Xie et al., 2018). Quantitative PCR showed that intrathecal injection with VTX (100 ng) increased the mRNA expression of TNF-α, IL-1β, IL-6, and CCL2, but not CXCL1 in WT mice, and the expression of TNF-α, IL-1β, and CCL2 was substantially inhibited in *Tlr8*^{-/-} mice (Fig. 6 G), indicating that VTX-induced expression of TNF-α, IL-1β, and CCL2 is dependent on TLR8 in the DRG.

Next, we checked ERK activation and inflammatory mediators' expression in the L5 DRG after SNL. We first examined whether ERK is activated in TLR8⁺ neurons after SNL. Double staining of TLR8 and pERK showed a high colocalization at days 3, 10, and 21 (Fig. 6 H). At day 10, 91.4 ± 2.8% of TLR8⁺ neurons expressed pERK, and 66.7 ± 1.7% of pERK⁺ neurons expressed TLR8 (Fig. 6 I). Western blotting confirmed the increase of pERK in WT mice 10 d after SNL. However, pERK was not significantly increased in *Tlr8*^{-/-} mice (Fig. 6 J). Furthermore, the expression of TNF-α, IL-1β, and CCL2 was increased in the DRG of WT mice 10 d after SNL, and the level of IL-1β and CCL2 was mostly reduced in *Tlr8*^{-/-} mice (Fig. 6 K). These data suggest that TLR8 is involved in ERK activation and inflammatory mediators' production in neuropathic pain condition.

VTX increases neuronal excitability of DRG neurons

Neuronal hyperexcitability of DRG is correlated with neuropathic pain (Zhang et al., 1997; Song et al., 2008), and ERK and inflammatory mediators regulate DRG neuronal excitability (Jin and Gereau, 2006; Stamboulian et al., 2010; Belkouch et al., 2011). We then checked if TLR8 is involved in the increased neuronal excitability after SNL. We compared evoked action potentials (APs) of DRG neurons in WT and *Tlr8*^{-/-} mice 10 d after SNL. In responding to 100, 200, and 300 pA ramp current stimula-

The total number of scratches in 30 min following intradermal injection of VTX in the nape. $n = 6$ mice per group. $P > 0.05$. One-way ANOVA followed by post hoc Bonferroni's test. Veh, vehicle. Data are representative of three independent experiments. (I) Double immunostaining shows that TLR8 is colocalization with TuJ1 (a marker for nerve fibers) in paw glabrous skin. (K) Double immunostaining of TLR8 and TuJ1 in nape hairy skin. Bar, 50 µm.



tion, the APs were dramatically increased in WT mice after SNL (**Fig. 7, A and B**), but were not significantly changed in *Tlr8*^{-/-} mice (**Fig. 7, C and D**). To further determine if VTX is sufficient to increase the excitability of DRG neurons, the whole mount DRG was incubated with vehicle or VTX (500 nM) for 30 min. In responding to 100, 200, and 300 pA ramp current stimulation, the number of APs was significantly increased in DRG neurons from WT mice (**Fig. 7, E and F**). However, VTX treatment did not change the number of APs in DRG from *Tlr8*^{-/-} mice (**Fig. 7, G and H**), and it still increased APs in the DRG from *Tlr7*^{-/-} mice (**Fig. 7, I and J**).

To examine whether ERK is involved in TLR8-mediated enhancement of neuronal excitability, the DRGs were preincubated with PD98059 (20 μ M), an ERK inhibitor 30 min before VTX. PD98059 inhibited VTX-induced increase of APs (**Fig. 7, K and L**), suggesting that ERK activation is essential for the increase of neuronal excitability induced by VTX. These data indicate that VTX increases neuronal excitability of DRG via TLR8/ERK signaling.

miR-21 expression is increased in DRG neurons after SNL

As miR-21 and miR-29a were reported to be secreted from tumor and bind as ligands to human TLR8 in immune cells ([Fabbri et al., 2012](#)), we asked if TLR8 can be activated by miRNA in the mouse DRG. We first checked the DRG expression of miR-21 and miR-29a in C57BL/6 mice. Quantitative PCR showed that miR-21 was dramatically (more than fivefold) increased at days 1, 3, and 10 after SNL, whereas miR-29a was only increased 10 d after SNL with a more than twofold increase (**Fig. 8 A**). We then focused on miR-21 for further studies.

The *in situ* hybridization showed that miR-21 was constitutively expressed in naive DRG (15 \pm 2%) of C57BL/6 mice. SNL increased the percentage of miR-21 positive cells to 41 \pm 2% at day 10 after SNL (**Fig. 8, B, D, and E**). Furthermore, cell profiling showed that miR-21 was expressed in neurons of all sizes 10 d after SNL (**Fig. 8 C**). The *in situ* hybridization for mature miR-21 (mmu-miR-21-5p) combined with immunostaining for TLR8 showed that miR-21 was colocalized with TLR8 in small- and medium-sized neurons, but not in large neurons (**Fig. 8, E-G**). Statistical analysis showed that 49.6% of miR-21⁺ neurons expressed TLR8, and 71.8% of TLR8⁺ neurons expressed miR-21 (**Fig. 8 H**).

miR-21 induces TLR8-dependent mechanical allodynia, ERK activation, inflammatory responses, and neuronal hyperexcitability

To evaluate whether miR-21 induces pain hypersensitivity via TLR8, we intrathecally injected miR-21 (5 μ g) in WT and *Tlr8*^{-/-} mice. miR-21 decreased paw withdrawal threshold at 3 h in WT mice, but not in *Tlr8*^{-/-} mice (**Fig. 8 I**). Also, miR-21 increased pPERK expression in the DRG of WT mice, but not in *Tlr8*^{-/-} mice (**Fig. 8 J**). The same treatment of miR-21 did not change pNF κ B

expression in WT mice (**Fig. S5, A and B**). The ERK or NF κ B luciferase reporter assay also showed that miR-21 induced ERK, but not NF κ B activation (**Fig. S5, C and D**).

We then checked the expression of inflammatory mediators in the DRG after miR-21 intrathecal injection. As shown in **Fig. 8 K**, miR-21 increased the expression of TNF- α , IL-1 β , IL-6, CCL2, and CXCL1 in WT mice. In *Tlr8*^{-/-} mice, the mRNA expression of these inflammatory mediators was substantially decreased compared with WT mice (**Fig. 8 K**). These data suggest that miR-21-induced inflammatory response is dependent on TLR8 in the DRG.

We further recorded neuronal excitability of the whole mount DRG. Incubation of DRG with miR-21 (10 μ M; [Park et al., 2014](#)) markedly increased the number of APs in the DRG neurons from WT mice, whereas miR-21 did not change the number of APs in the DRG from *Tlr8*^{-/-} mice (**Fig. 8, L and M**), indicating that miR-21 increases neuronal excitability via TLR8.

Inhibition of miR-21 alleviates neuropathic pain

To assess whether miR-21 contributes to the development of neuropathic pain, we injected antagonim-21 into the L5 spinal nerve after SNL. Behavioral study showed that low dose of the antagonim-21 (0.3 μ g) did not affect the paw withdrawal threshold, but the high dose (0.5 μ g) antagonim-21 gradually increased the threshold and attenuated mechanical allodynia at day 4 (**Fig. 8 N**). These data indicate that miR-21 is involved in the maintenance of neuropathic pain.

Discussion

Innate receptors such as TLRs, C-type lectin receptors, NOD-like receptors, and RIG-I-like receptors (RLRs) have been widely investigated in the immune system as they recognize microbial pathogens and play an essential role in the initiation of innate immune responses ([Kawai and Akira, 2011](#)). Besides a few NOD-like receptors, such as NLRP3 and NOD2, which have been reported to be involved in neuropathic pain ([Grace et al., 2016](#); [Santa-Cecilia et al., 2018](#)), the role of TLRs in pain has been widely investigated ([Liu et al., 2012b](#); [Ji, 2015](#)). For example, *Tlr2* knock-out mice show delayed and reduced mechanical allodynia and heat hyperalgesia after L5 spinal nerve transection ([Kim et al., 2007](#)). TLR9 antagonist blocked tumor-induced pain sensitivity ([Qi et al., 2011](#)). *Tlr4* deletion or inhibition by antagonist or siRNA attenuated arthritic pain ([Christianson et al., 2011](#)) and bone cancer pain ([Wu et al., 2010](#)). Different from these TLRs, *Tlr7* deletion did not affect inflammatory pain and neuropathic pain, but reduced nonhistaminergic itch ([Liu et al., 2010](#)). TLR8, as homologous to TLR7, is less investigated than TLR7 in the function of pain and itch. We provide the first evidence that TLR8 and TLR7 have different cellular distribution in the DRG, and *Tlr8* de-

Figure 5. The subcellular localization of TLR8 in DRG neurons. **(A)** Confocal images show that TLR8 is distributed as punctuate structures in the cytoplasm of DRG neuron. Bar, 5 μ m. **(B)** Double immunostaining of TLR8 and EEA1 in DRG neurons of naive mice and SNL mice. **(C)** Statistical data shows the percentage of the area of TLR8/EEA1 costaining in the area of the cytoplasm. *, P < 0.05, Student's unpaired t test. **(D)** Double immunostaining of TLR8 and LAMP1 in DRG neurons of naive mice and SNL mice. **(E)** Statistical data shows the percentage of the area of TLR8/LAMP1 costaining in the area of the cytoplasm. *, P < 0.05, Student's unpaired t test. **(F)** Double immunostaining of TLR8 and calnexin in DRG neurons of naive mice and SNL mice. Bar, 10 μ m. **(G)** Statistical data shows the percentage of the area of TLR8/calnexin costaining in the area of the cytoplasm. *, P < 0.05, Student's unpaired t test. Data are representative of three independent experiments.

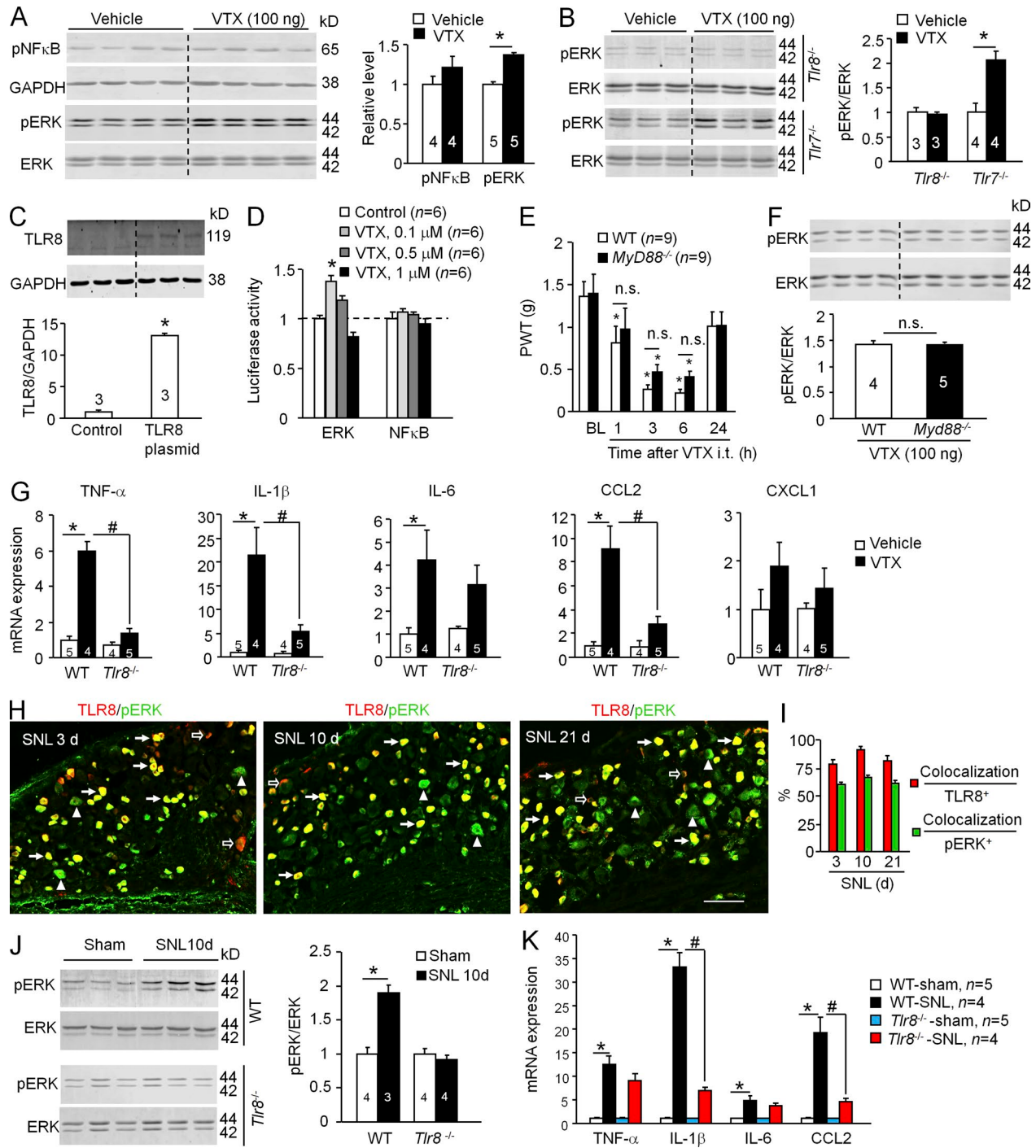


Figure 6. *Tlr8* deletion decreases the ERK phosphorylation and inflammatory mediator expression induced by VTX or SNL. **(A)** Western blotting shows that intrathecal injection of VTX increased the pERK expression, but did not affect the expression of pNF κ B in the DRG. $n = 4-5$ mice per group. *, $P < 0.05$ compared with vehicle group. Student's unpaired t test. Data are representative of two independent experiments. **(B)** Western blotting shows that the increase of pERK expression induced by VTX was abrogated in *Tlr8 $^{-/-}$* mice, but not affected in *Tlr7 $^{-/-}$* mice. $n = 3-4$ mice per group. *, $P < 0.05$ compared with vehicle group. Student's unpaired t test. Data are representative of two independent experiments. **(C)** Western blotting shows TLR8 expression in HEK293 cells 24 h after TLR8 plasmid transfection. $n = 3$ cultures per group. *, $P < 0.05$ compared with control group. Student's unpaired t test. **(D)** Luciferase assay shows the firefly activity in HEK293 cells cotransfected with pNF κ B-luc (or pGL4.33) plasmid and TLR8 plasmid after VTX stimulation for 12 h. $n = 6$ cultures per group. $P > 0.05$. One-way ANOVA followed by post hoc Bonferroni's test. Data are representative of three independent experiments. **(E)** VTX reduced paw withdrawal threshold in WT and *Myd88 $^{-/-}$* mice. $n = 9$ mice per group. *, $P < 0.05$ compared with baseline (BL). One-way ANOVA followed by post hoc Bonferroni's test. n.s., not significant; $P > 0.05$. Two-way ANOVA followed by post hoc Bonferroni's test. Data are representative of two independent experiments. **(F)** Western blotting analysis shows the expression of pERK and ERK in the DRG after VTX intrathecal injection in WT and *Myd88 $^{-/-}$* mice. $n = 4-5$ mice per group. n.s., not significant. $P > 0.05$. Student's unpaired t test. Data are representative of two independent experiments. **(G)** Quantitative PCR shows the effect of VTX on the expression of cytokines and chemokines in the DRG of WT and *Tlr8 $^{-/-}$* mice. $n = 4-5$ mice per group. *, $P < 0.05$ compared with the vehicle group. #, $P < 0.05$ compared with the WT-VTX mice. Student's unpaired t test. **(H)** Double staining of TLR8 and pERK in the DRG after SNL. Filled arrows show the typical

ficiency markedly attenuated neuropathic pain induced by SNL or PTX in mice. Especially, SNL-induced mechanical allodynia was fully recovered at day 21 in *Tlr8*^{-/-} mice, although it can be maintained for >3 mo in WT mice (Jiang et al., 2016). Taken with the reversal effect of *Tlr8* siRNA on SNL-induced mechanical allodynia, these data suggest an important and distinct role of TLR8 in mediating neuropathic pain.

The involvement of certain TLRs in pain and itch is closely correlated with the cellular expression in the nervous system. Microglia and astrocytes were shown to express various TLRs, including TLR2 and TLR4 (Bsibsi et al., 2002). Accordingly, nerve injury-induced spinal microglia and astrocyte activation is reduced in the *Tlr2* or *Tlr4* knock-out mice (Kim et al., 2007; Christianson et al., 2011). Dry skin-induced chronic itch and astrocyte activation are also reduced in *Tlr4* knock-out mice (Liu et al., 2016). The reduced spinal activation of astrocytes and microglia after SNL is consistent with the reduced neuropathic pain hypersensitivity in *Tlr8*^{-/-} mice. As TLR8 was mainly expressed in small DRG neurons, which gave rise to unmyelinated axons (C-fibers) and thinly myelinated axons (A δ -fibers) and mediated noxious signal transmission to the spinal cord, it is likely that the decreased glial activation in *Tlr8*^{-/-} mice is due to an indirect effect, such as the reduced excitatory input from the DRG (Fig. 7). However, *Tlr8* mRNA increase (3 d) was not as early as the induction (1 d) of neuropathic pain (Zhang et al., 2013), and SNL-induced pain hypersensitivity was not affected in early days in *Tlr8*^{-/-} mice, suggesting that TLR8 may play an essential role in the maintenance of neuropathic pain. Other TLRs, such as TLR4 or TLR2, may be responsible for the development of neuropathic pain (Tanga et al., 2005; Li et al., 2015).

Although inhibition of TLR8 attenuated both mechanical allodynia and heat hyperalgesia, intrathecal injection VTX-2337 induced only mechanical allodynia, which may be due to the predominant expression of TLR8 in IB4-binding neurons. Previous studies suggest that IB4-binding neurons play particular roles in mediating the behavioral responses to mechanical stimuli (Cavanaugh et al., 2009; Barabas et al., 2012). For example, genetic ablation G-protein coupled receptor Mrgprd, which is expressed in ~80% IB4-binding neurons (Zylka et al., 2005), caused specific deficits in the behavioral response to noxious mechanical stimuli, but not to heat stimuli (Cavanaugh et al., 2009). TRPA1, a plasma membrane ion channel that contributes to mechanical and cold hypersensitivity during tissue injury, is also mainly distributed in IB4-binding neurons in mice (Barabas et al., 2012). We also found that intraplantar injection of VTX-2337 induced spontaneous pain, indicating that activation of TLR8 is sufficient to induce pain hypersensitivity.

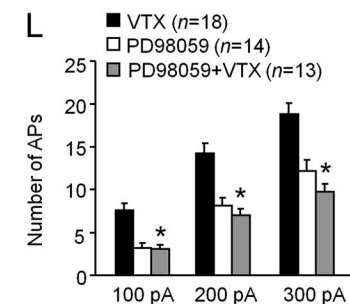
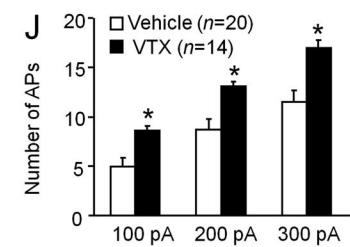
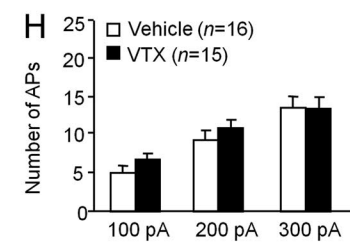
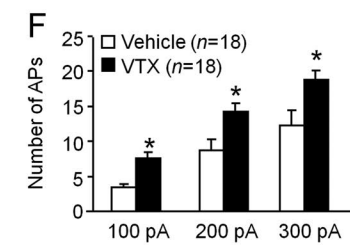
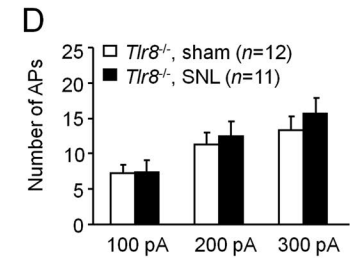
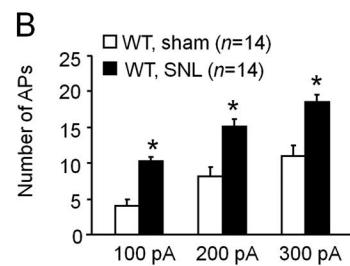
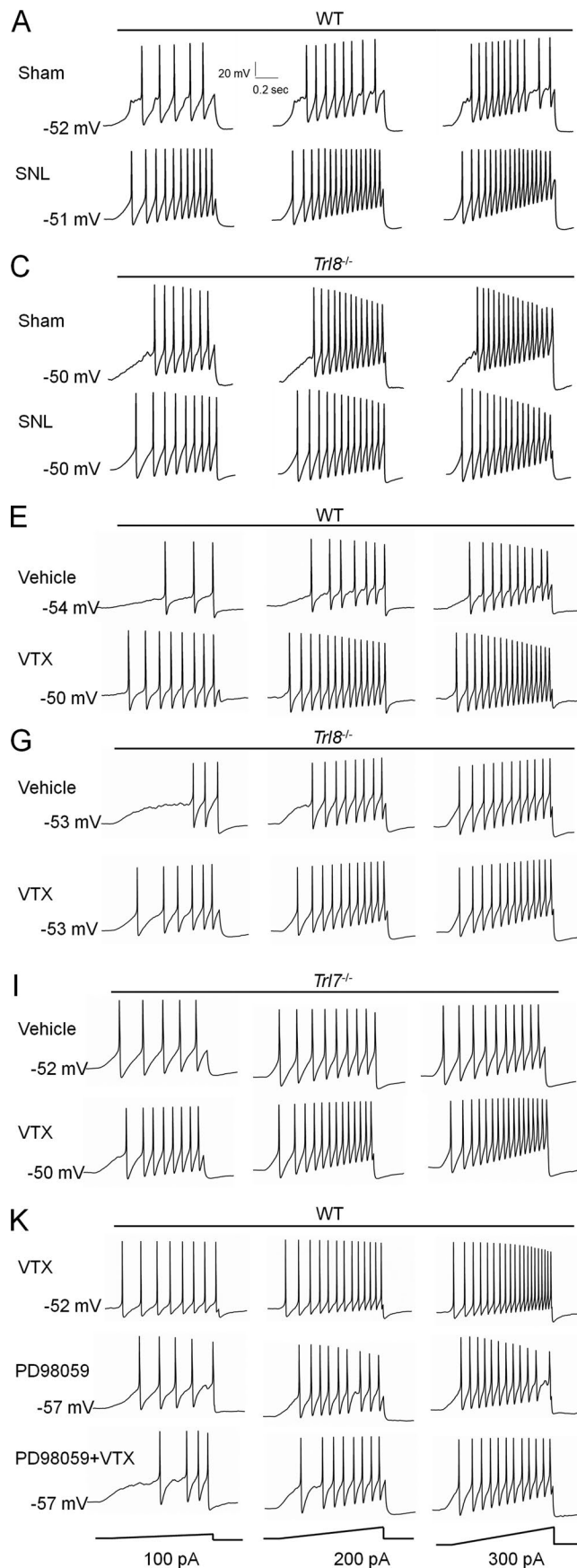
TLR3 and TLR7 are localized on membrane and in intracellular compartments depending on cell type and conditions (Akira et al., 2006). In cortical and hippocampal neurons, TLR7 is ex-

pressed on endosomal membrane (Lehmann et al., 2012). However, in DRG neurons, TLR7 is expressed on plasma membrane (Park et al., 2014). The localization of TLR8 in the ER, endosomes, and lysosomes of DRG neurons is the same as that in human monocytes and macrophages (Itoh et al., 2011; Ishii et al., 2014). It was reported that UNC93B1, an ER-resident membrane protein, mediates the trafficking of TLRs (TLR3, TLR7, TLR8, and TLR9) from the ER to endolysosomes (Lee et al., 2013). Thus, TLR8 in the ER may be transported via UNC93B1 to the endosomes and lysosomes to exert functions.

The canonical downstream signaling of intracellular TLRs (except for TLR3) is to induce MyD88-mediated NF κ B activation and subsequent induction of cytokine expression (Akira and Takeda, 2004; Liu et al., 2012b; Sarvestani et al., 2012), and NF κ B activation has been used to monitor TLRs function in most early experiments (Jurk et al., 2002; Demaria et al., 2010). However, our data support ERK, but not NF κ B, as a downstream kinase of TLR8 in DRG neurons. In addition, MyD88 is not necessary for TLR8-induced ERK activation. Differently, VTX-2337 activated NF κ B phosphorylation in human monocytes and myeloid dendritic cells and HEK293 (Lu et al., 2012), and MyD88 is essential for TLR8 activation in human monocytes and macrophages (Bergström et al., 2015; Krüger et al., 2015) and murine dendritic cells (Martinez et al., 2010). However, NF κ B and MyD88 are not involved in TLR8 activation in mouse cortical neurons (Ma et al., 2007). We postulate that the downstream signaling of TLR8 in neurons may be different from that in immune cells, which needs to be further investigated on human neurons in the future.

TLR-mediated inflammation plays a critical role in mediating inflammatory responses in the immune system (Liu et al., 2012b). Cytokines, including TNF- α , IL-1 β , and IL-6 (Xu et al., 2006; Kawasaki et al., 2008), and chemokines, including CCL2 and CXCL1, have been implicated in the pathogenesis of chronic pain (Gao et al., 2009; Zhang et al., 2013). Our results demonstrated that ERK and TNF- α , IL-1 β , and CCL2 are the downstream signaling of TLR8 in the DRG. It has been well demonstrated that ERK is activated in the DRG after tissue inflammation or nerve injury (Obata et al., 2004a,b). ERK also mediates nerve injury-induced TNF- α and IL-1 β increase in trigeminal neurons (Zhang et al., 2016). Accumulating evidence supports that ERK and inflammatory mediators increase excitability of DRG neurons. For example, ERK acutely regulates DRG neuron excitability via direct phosphorylation and modulation of Nav1.7 (Stamboulian et al., 2010). TNF- α rapidly enhances tetrodotoxin-resistant sodium currents in isolated DRG neurons (Jin and Gereau, 2006). CCL2 excites primary sensory neurons by increasing Nav1.8 activity in DRG neurons (Belkouch et al., 2011). In addition, IL-1 β increases the excitability of IB4-positive DRG neurons via activating ERK (Stemkowski and Smith, 2012). Thus, TLR8-mediated activation

double-labeled neurons; blank arrows show the typical TLR8 single labeled neurons; arrowheads show the typical pERK single labeled neurons. Bar, 100 μ m.
(I) Statistical data show the percentage of double-labeled neurons. **(J)** Western blotting shows that the pERK expression was increased in WT mice, but not in *Tlr8*^{-/-} at SNL 10 d. $n = 3\text{--}4$ mice per group. *, $P < 0.05$ compared with the sham group. Student's unpaired *t* test. Data are representative of two independent experiments. **(K)** Quantitative PCR shows the expression of cytokines and chemokines in the DRG of WT and *Tlr8*^{-/-} mice after SNL. Data are representative of two independent experiments. $n = 4\text{--}5$ mice per group. *, $P < 0.05$ compared with the WT-sham group. #, $P < 0.05$ compared with WT-SNL mice. Student's unpaired *t* test.



of ERK and production of TNF- α , IL-1 β , and CCL2 may form a positive feedback loop to increase neuronal excitability and further contribute to neuropathic pain.

miRNAs are small, noncoding RNAs, 19–24 nt in length. They can negatively regulate gene expression by canonical binding to their target mRNAs or directly interact with proteins. TLR8 and TLR7 can recognize and bind not only exogenous viral or bacterial ssRNA, but also endogenous miRNAs (Liu et al., 2012b). Recent array studies showed that nerve injury changes the expression of a variety of microRNAs in the DRG. Among them, miR-21 expression is consistently shown to be increased (Strickland et al., 2011; Li et al., 2012; Sakai et al., 2013). Strickland et al. (2011) reported that miR-21 is expressed in DRG neurons of all sizes, and colocalized with NF200 and CGRP. The function study shows that continuous infusion of miR-21 inhibitor attenuated SNL-induced pain hypersensitivity in rats (Sakai and Suzuki, 2013), but the underlying mechanism was not investigated. We confirmed the role of miR-21 on TLR8-dependent activation of ERK, production of inflammatory mediators in the DRG. Although miR-21 and TLR8 are only colocalized in small- and medium-diameter neurons, miR-21 may be secreted from large neurons and reach TLR8 in endosomes of other neurons (Fabbri et al., 2012).

The previous study showed that TLR7 is activated by miRNA let-7b in cortical neurons and DRG neurons (Lehmann et al., 2012; Park et al., 2014). Furthermore, the GUUGUGU motif is essential for the activation of TLR7, as this motif-containing let-7b and miR-599 induce TLR7/TRPA1-dependent inward currents and action potentials in DRG neurons (Park et al., 2014). In contrast, miR-21 and miR-29a did not activate TLR7/TRPA1 signaling (Park et al., 2014). Fabbri et al. (2012) reported that miR-21 and miR-29a increased TLR8 activation in TLR8-HEK293 cells. A recent study demonstrated that human TLR8 recognize two degradation products of ssRNA: uridine and a short oligonucleotide, and both binding sites were essential for activation of TLR8 by ssRNA (Tanji et al., 2013). Future studies to clarify the specific sequences of ssRNA that required for the activation of TLR8 in the DRG are needed.

In conclusion, we provide the first demonstration that TLR8, different from TLR7, plays a pivotal role in the maintenance of neuropathic pain. In addition, miR-21 may operate as an endogenous ligand, acts on TLR8 in endosomes and lysosomes, induces ERK activation and inflammatory mediators' production, further increases neuronal excitability, and contributes to the maintenance of neuropathic pain. Notably, TLR8 is not only expressed in small-sized DRG neurons in mice, but also in human (Fig. S4), and *Tlr8* siRNA effectively attenuated neuropathic pain in mice. Thus, TLR8 may be a promising target for the treatment of neuropathic pain.

Materials and methods

Animals and surgery

Adult ICR mice and C57BL/6 were purchased from the Experimental Animal Center of Nantong University (Jiangsu, China). *Tlr8*^{-/-} mice (C57BL/6 background) were generated by CAYN Company. *Tlr7*^{-/-} mice (B6.129S1-Tlr7tm1Flv/J; stock no. 008380; C57BL/6 background) were purchased from Jackson Laboratory. *MyD88*^{-/-} mice (C57BL/6 background) was purchased from Model Animal Research Center of Nanjing University. All animal procedures performed in this study were reviewed and approved by the Animal Care and Use Committee of Nantong University. To produce SNL, animals were anesthetized with isoflurane, and the L6 transverse process was removed to expose the L4 and L5 spinal nerves. The L5 spinal nerve was then isolated and tightly ligated with 6-0 silk thread (Zhang et al., 2013). For sham operations, the L5 spinal nerve was exposed, but not ligated.

Generation of transcription activator-like effector nuclease-mediated *Tlr8*^{-/-} mice

TALENs were used to create *Tlr8*^{-/-} mice (GenBank accession no. NM_001313760.1). TALENs were designed to target exon 2 of *Tlr8* using the TALENdesigner software (TALEs-L: 5'-TGC CATCTCCATAAAGC-3'; spacer: 5'-GAACATTCCAGAAC-3'; TALEs-R: 5'-TATCCTTGACGAGATA-3'). TALEN mRNAs were generated by in vitro transcription and injected into fertilized eggs of C57BL/6. The binding of TALENs with the *Tlr8* genome loci induced a site-specific double-strand break followed by nonhomologous end joining repair, resulting in the deletion of some bases. The chimera mice were identified by DNA sequencing (primer: 5'-GTAATGGCATTGTCTGACAAGTCTATG-3'). Male chimeric mice were mated to C57BL/6 mice, and heterozygous TLR8 mice (*Tlr8*^{+/-}) were intercrossed to generate *Tlr8*^{-/-} mice and WT littermates.

Drugs and administration

Histamine, Compound 48/80, CQ, and R848 were purchased from Sigma-Aldrich. Imiquimod and loxoribine were purchased from InvivoGen. These reagents were intradermally injected into the nape. Formalin, capsaicin, and CFA were purchased from Sigma-Aldrich, and were intraplantarly injected. Paclitaxel was purchased from Aladin and was intraperitoneally injected (6 mg/kg). VTX-2337 was purchased from Active Biochem. TLR8 siRNA, miR-21 mimic, and miR-21 antagonist were synthesized by RiboBio. The sequences are shown in Table S1. Intrathecal injection was made with a 30-G needle between the L5 and L6 intervertebral spaces to deliver the reagents to the cerebrospinal fluid (Hylden and Wilcox, 1980). For peri-spinal nerve injection, TLR8 siRNA (2 μ g) was mixed with RVG-9R peptide (molar ratio siRNA/RVG-9R = 1:10; Anaspec; Berta et al., 2014), and then in-

Figure 7. SNL- and VTX-induced increase of the APs in DRG neurons is blocked by *Tlr8* deletion. (A and C) Examples of membrane potential traces evoked by current injection in neurons dissected 10 d after sham-operation or SNL in WT (A) or *Tlr8*^{-/-} (C) mice. **(B and D)** Histogram shows the number of APs in WT (B) or *Tlr8*^{-/-} (D) mice. $n = 11\text{--}14$ neurons/group. *, $P < 0.05$, compared with sham group; Student's unpaired *t* test. **(E, G, and I)** The representative traces of APs from DRG neurons of WT mice (E), *Tlr8*^{-/-} (G), or *Tlr7*^{-/-} mice (I) in response to drugs (vehicle, VTX). **(F, H, and J)** Histogram shows the number of APs in response to drugs. $n = 14\text{--}20$ neurons per group. *, $P < 0.05$ compared with the vehicle group; Student's unpaired *t* test. **(K)** The representative traces of APs from DRG neurons of WT mice treated with PD98059 and VTX. **(L)** Histogram shows the number of APs in response to drugs. $n = 13\text{--}18$ neurons per group. *, $P < 0.05$, compared with VTX group; one-way ANOVA followed by post hoc Bonferroni's test.

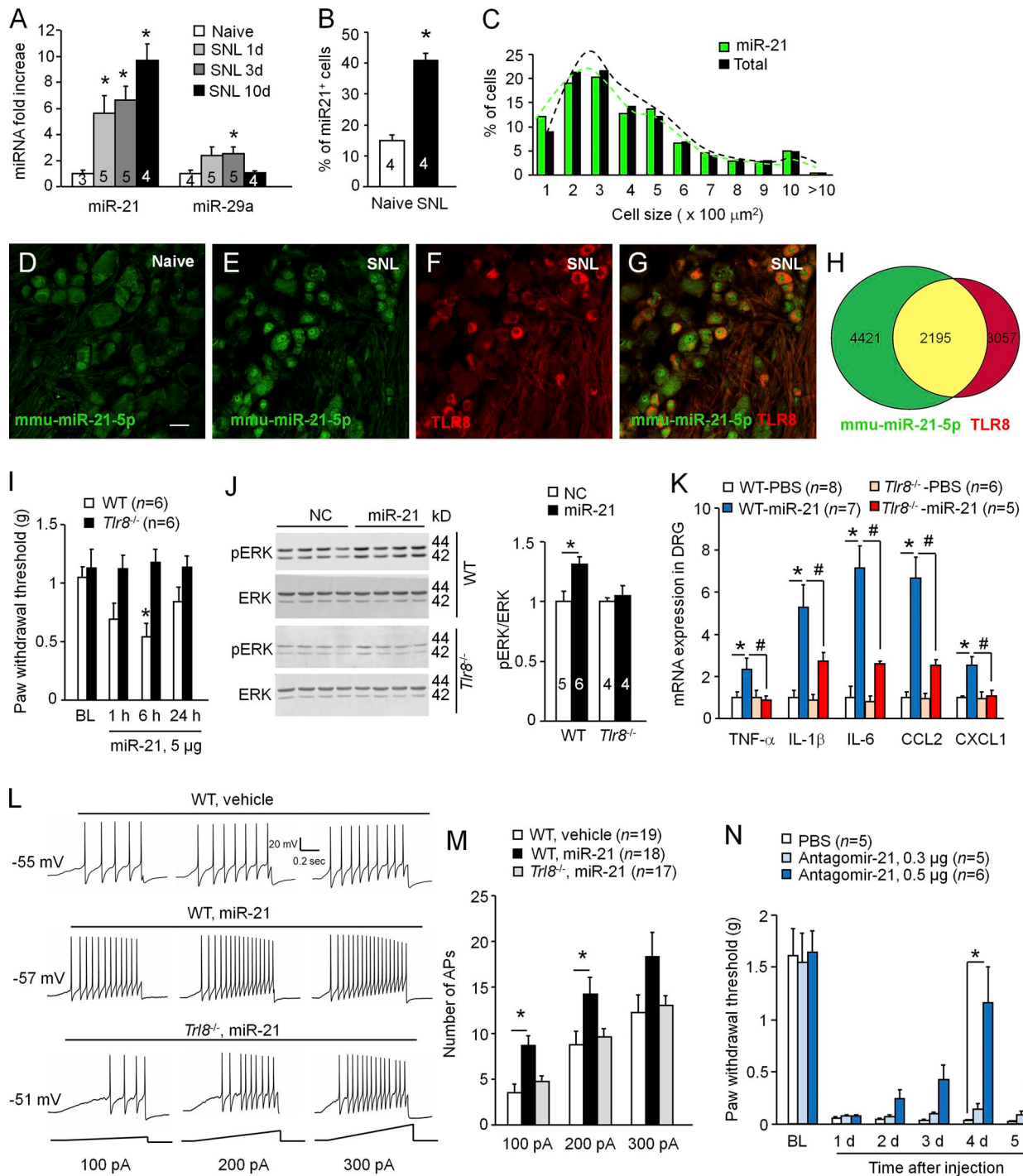


Figure 8. miR-21 acts on TLR8 to increase pERK expression, inflammatory mediator expression, and neuronal excitability in the DRG. **(A)** Quantitative PCR shows the expression of miR-21 and miR-29a in DRG following SNL. Data are representative of two independent experiments. $n = 3\text{--}5$ mice per group. *, $P < 0.05$ compared with the naive group; one-way ANOVA followed by post hoc Bonferroni's test. **(B)** The percentage of miR-21 positive neurons in the total of DRG neurons in naive and SNL mice. $n = 4$ mice per group. *, $P < 0.05$ compared with the naive group; Student's unpaired *t* test. **(C)** The cell size distribution frequency of miR-21 positive neurons and total neurons in the DRG of SNL 10 d mice. **(D)** In situ hybridization shows the cellular distribution of miR-21 on DRG sections from naive mice. Bar, 25 μm . **(E and G)** In situ hybridization combining with immunostaining shows the colocalization of miR-21 and TLR8 in the DRG of SNL 10 d mice. **(H)** The Venn diagrams showing the colocalization of miR-21⁺ neurons with TLR8⁺ neurons. **(I)** Intrathecal injection of miR-21 reduced the paw withdrawal threshold in WT mice, but not in *Tlr8^{-/-}* mice. Data are representative of three independent experiments. $n = 6$ mice per group. *, $P < 0.05$ compared with corresponding baseline. Two-way RM ANOVA followed by post hoc Bonferroni's test. **(J)** Intrathecal injection of miR-21 increased pERK expression in DRG tissues from WT mice, but not *Tlr8^{-/-}* mice. Data are representative of two independent experiments. $n = 4\text{--}6$ mice per group. NC, negative control miRNA. *, $P < 0.05$ compared with the NC group; Student's unpaired *t* test. **(K)** Quantitative PCR shows that intrathecal injection of miR-21 increased the expression of cytokines and chemokines in the DRG of WT mice, which was reduced in *Tlr8^{-/-}* mice. $n = 5\text{--}8$ mice per group. *, $P < 0.05$ compared with WT-PBS group. #, $P < 0.05$ compared with the WT-miR-21 group. One-way ANOVA followed by post hoc Bonferroni's test. **(L)** The representative traces of APs from DRG neurons of WT and *Tlr8^{-/-}* in response to vehicle and miR-21. **(M)** Histogram shows the number of APs from DRG neurons of WT and *Tlr8^{-/-}* in response to vehicle and

jected into L5 spinal nerve. The scrambled siRNA was used as a control. miR-21 antagonist was dissolved in PBS and injected the same way as *Tlr8* siRNA.

Pain behavior analysis

Animals were habituated to the testing environment daily for at least 2 d before baseline testing. For the von Frey test, the animals were put in boxes on an elevated metal mesh floor and allowed 30 min for habituation before the examination. The plantar surface of the hind paw was stimulated with a series of von Frey hairs with logarithmically incrementing stiffness (0.02–2.56 g; Stoelting). The 50% paw withdrawal threshold was determined using Dixon's up-down method (Dixon, 1980). For the Hargreaves test, the animals were put in a plastic box placed on a glass plate, and the plantar surface was exposed to a beam of radiant heat through a transparent glass surface (Life Science). The baseline latencies were adjusted to 10–14 s with a maximum of 20 s as a cutoff to prevent potential injury (Hargreaves et al., 1988). All the behavioral experimenters were done by individuals that were blinded to the treatment or genotypes of the mice.

Itch behavior analysis

The back of the neck was shaved 2 d before experiments. On the day of behavioral testing, mice were individually placed in small plastic chambers and allowed at least 30 min for habituation. Under brief anesthesia with isoflurane, mice were given an intradermal injection of 50 μ l of reagents via a 30-G needle into the nape of the neck. Immediately after the injection, mice were returned to the chambers and recorded for 30 min. The video was subsequently played back offline, and the scratching behavior was quantified in a blinded manner. A scratch was counted when a mouse lifted the hind paw to scratch the shaved skin and returned the paw to the floor or mouth (Liu et al., 2016).

RNA isolation and quantitative real-time PCR for mRNAs and microRNAs

The total RNA was extracted by applying TRIzol reagent (Invitrogen) according to the manufacturer's protocol. Each L5 or L4 DRG RNA sample was a mixture of mRNAs from three mice under the same treatment. Immediately after isolation, RNA quantity and quality was determined by using a NanoDrop spectrophotometer (Thermo Fisher Scientific). 1 μ g of total RNA was reversely transcribed using the First Strand cDNA Synthesis kit (Takara). For microRNA detection, small RNAs were extracted using RNAiso kit (Takara), and 10 ng of small RNA was reversely transcribed into cDNA using the One Step PrimeScript microRNA cDNA Synthesis kit (Takara) according to manufacturer's instructions. Quantitative PCR analysis was performed in the Real-time Detection System (Rotor-Gene 6000) by SYBR Premix Ex Taq II kit (Takara). The sequences of primers are shown in Table S2. The PCR amplifications were performed at 95°C for 30 s, followed by 40 cycles of thermal cycling at 95°C for 5 s and 60°C for 45 s.

Data were collected after each cycle and displayed graphically (Rotor-Gene 6000 Series Software 1.7). GAPDH and U6 small nuclear RNA were used as endogenous control to normalize differences for mRNA and microRNA detection, respectively. Melt curves were performed upon completion of the cycles to ensure that nonspecific products were absent. Quantification was performed by normalizing target gene cycle threshold (C_t) values with corresponding GAPDH C_t (mRNA) or U6 C_t (microRNA), and then analyzed with the $2^{-\Delta\Delta C_t}$ method.

DRG neuron culture

After anesthesia with isoflurane, the bilateral lumbar DRGs in mouse (4–6 wk old) were rapidly removed (Lee et al., 2014). The connective tissues and meninges were carefully stripped in an ice-cold oxygenated balanced salt solution (BSS in mM: 125 NaCl, 3 KCl, 26 NaHCO₃, 1.25 NaH₂PO₄, 10 glucose, 2.4 CaCl₂, 1.2 MgCl₂, 5 Hepes, pH 7.2, and osmolarity: 300 mOsm), and each DRG was minced with scissors. These DRG tissues were incubated with oxygenated artificial cerebrospinal fluid (aCSF), which contained collagenase (3.0 mg/ml, Roche) and dispase-II (2.4 U/ml, Roche) at 37°C for 90 min, and then washed with standard aCSF. Neurons were mechanically dissociated using a set of various flame-polished glass pipettes and plated onto poly-D-lysine-coated glass coverslips (diameter, 13 mm). The dissociated DRG neurons were plated on poly-ornithine-laminin-coated glass coverslips and incubated in aCSF at 37°C (humidified 95% O₂ and 5% CO₂). 24 h later, neurons were used for single-cell RT-PCR.

Single-cell RT-PCR

After DRG neurons adhered to the glass coverslips, IB4-conjugated with FITC (1:200) was incubated with these neurons for 1 h to distinguish the IB4⁺ and IB4⁻ neurons. The protocol of single-cell RT-PCR was performed as previously described (Liu et al., 2012a). In brief, the single cell was aspirated into a glass pipette with a tip diameter of ~25 μ m, and then gently pushed into a reaction tube containing the reverse transcription reagents. The first reaction was performed at 37°C for 40 min and then at 80°C for 10 min to remove the genomic DNA (Invitrogen). The reverse transcription reaction was then performed at 50°C for 50 min and 70°C for 15 min. The harvested cDNA product was used in separate PCR. The sequences of the single-cell PCR primers used are presented in Table S3. The first round of PCR was performed in 10 μ l of PCR buffer containing "outer" primers of *Tlr8*, *Tlr7*, *NeuN*, and *Gapdh*, respectively. The amplification condition of PCR included an initial 5 min denaturing step at 95°C followed by 30 cycles of 40 s denaturation at 95°C, 40 s annealing at 58°C, and 40 s elongation at 72°C. The reaction was completed within 7 min of final elongation. The products of this step were diluted for 1,000-fold and further amplified. The second round of PCR was performed in 10 μ l of PCR buffer with the corresponding "inner" primers. The amplification condition was the same as the first round of PCR. A negative control was obtained from pipettes that

miR-21. $n = 17$ –19 neurons per group. *, $P < 0.05$ compared with the vehicle group. One-way ANOVA followed by post hoc Bonferroni's test. (N) The peri-spinal nerve injection of antagonmir-21 dose-dependently attenuated the mechanical allodynia induced by SNL. Data are representative of two independent experiments. $n = 5$ –6 mice per group. *, $P < 0.05$ compared with the corresponding PBS group; two-way ANOVA followed by post hoc Bonferroni's test.

did not harvest any neuron contents but was submerged in the bath solution. The final PCR products were visualized by GelRed (Biotium) staining in 3% agarose gels.

HEK293 cell culture and transfection

HEK293 cells were cultured in high glucose DMEM (Bio Whitaker Europe) with 10% (vol/vol) fetal calf serum (PAA) and 0.5% penicillin/streptomycin at 37°C in a humidity-controlled incubator with 5% (vol/vol) CO₂. Cells were transfected with the appropriate plasmids using Lipofectamine 3000 (Invitrogen) at 80% confluence. Transfected cells were cultured in the same culture medium for 24 h or 12 h before Western blotting analysis or luciferase assay, respectively.

Luciferase reporter assays

HEK293 cells were transfected with plasmid mixture of pCMV TLR8 (Genechem) with pNFκB-luc (Beyotime) or pGL4.33 (luc2P/serum response element/hygro) vector (containing a serum response element that drives the transcription of the luciferase reporter gene luc2P in response to activation of MAPK-ERK signaling pathway; Promega). 48 h later, VTX was added, and the luciferase activity was measured by Dual-Luciferase Reporter Assay System (Promega).

Immunohistochemistry

Animals were deeply anesthetized with isoflurane and perfused through the ascending aorta with 0.01 M PBS followed by 4% paraformaldehyde in 0.01 M PBS. After the perfusion, the L5 spinal cord segment and DRG were removed and postfixed in the same fixative overnight. Spinal cord (30 μm; free floating) or DRG (15 μm) sections were cut in a cryostat and processed for immunofluorescence staining as we described previously (Gao et al., 2009). In brief, the sections were first blocked with 5% donkey serum for 2 h at room temperature, then incubated overnight at 4°C with the following primary antibodies: TLR8, CGRP, NF200, TLR7, EEA1, LAMP1, calnexin, PGP9.5, GFAP, NeuN, OX-42, IBA-1, pERK, TuJ1, CD68, and Nissl (see Table S4 for detailed information). The sections were then incubated for 2 h at room temperature with Cy3- or FITC-conjugated secondary antibodies. For double immunofluorescence, sections were incubated with a mixture of primary antibodies from different species followed by a mixture of FITC- and Cy3-conjugated secondary antibodies. IB4-FITC and Nissl-435 were mixed with fluorescence secondary antibody to do double staining. The stained sections were examined with a Leica fluorescence microscope (DM4000B) or Leica confocal microscope (SP8), and images were captured with a charge-coupled device Spot camera. Images were analyzed with National Institutes of Health ImageJ software or Adobe Photoshop.

Human DRG immunostaining

Non-diseased human DRG tissues are obtained from donors through National Disease Research Interchange. Postmortem L5 DRGs were fixed in 0.01 M PBS with 4% paraformaldehyde and 1.5% picric acid. DRG (15 μm) sections were cut in a cryostat and processed for immunostaining as above described. The double staining of TLR8 and peripherin was performed, and Nissl was given as a counterstaining.

In situ hybridization (ISH) of miR-21

Cellular localization of miR-21 in DRG was performed using the mature mouse miR-21 (mmu-miR-21a-5p) detection probe for ISH labeled by 5'- and 3'-FAM (Exiqon). In brief, animals were fixed via the ascending aorta with 0.1 M PBS containing 4% paraformaldehyde and 0.1% DEPC. DRGs were collected and then cut in a cryostat. DRG sections (15 μm) were treated with proteinase K (BosterBio) for 2 min at room temperature, and then washed in RNase-free PBS. After digestion with proteinase, sections were post-fixed with the 1% paraformaldehyde/PBS and then washed in DEPC-treated ultrapure water. Prehybridization procedures were performed under RNase-free conditions for 2 h at 40°C. Hybridization was performed with a hybridization probe specific to miR-21 at 42°C overnight in hybridization buffer (Jiang et al., 2016). Sections were then washed with 2× saline sodium citrate (SSC), 0.5× SSC, and 0.2× SSC buffers. The signal was detected with the Leica SP8 confocal microscope.

To identify the colocalization of miR-21 and TLR8, the above sections under miR-21 ISH were incubated overnight at 4°C with primary antibodies against TLR8. On the following day, a Cy3-conjugated secondary antibody was added and incubated for 2 h. The signal was detected with a Leica SP8 confocal microscope.

Western blotting

Animals were transcardially perfused with PBS, and the lumbar DRGs were dissected. DRGs were homogenized in a lysis buffer containing phosphatase and protease inhibitors (Sigma-Aldrich). Protein concentrations were determined by BCA Protein Assay (Thermo Fisher Scientific). Protein samples (30 μg) were separated on SDS-PAGE gel and transferred to PVDF membrane. The membrane was blocked with 5% milk and incubated overnight at 4°C with the following antibodies: pERK, ERK, pJNK, JNK, p-p38, p38, pNFκB, GAPDH, and TLR8 (Table S4). The membrane was further incubated with a HRP-conjugated secondary antibody, developed in ECL solution for 1–5 min. The membrane was scanned using the Chemidoc XRS system (Bio-Rad). Specific bands on the membrane were evaluated by apparent molecular size. The intensity of the selected bands was analyzed using ImageJ software.

The whole-mount DRG patch-clamp recording

Whole-mount DRGs were isolated using a protocol as described previously (Wu et al., 2016). In brief, the L4 and L5 DRGs were quickly removed from the vertebral column and placed in ice-cold aCSF solution saturated with 95% O₂ and 5% CO₂, that contains the following (in mM): 125 NaCl, 3 KCl, 2.4 CaCl₂, 1.2 MgCl₂, 1.25 NaH₂PO₄, 26 NaHCO₃, 11 glucose, and 5 Hepes, pH 7.4. The connective tissue was carefully removed under a microscope, and the ganglia were transferred to a 2-ml dissecting solution containing collagenase D (1.8 mg/ml; Roche) and trypsin (1 mg/ml; Ameresco) for 40 min at 37°C. The ganglia were taken from the enzyme solution, washed, and transferred into a holding chamber containing normal oxygenated aCSF in room temperature at least 1 h before recording.

The patch-clamp recording experiments were performed at room temperature, and the cells were continuously perfused with aCSF saturated with 95% O₂ and 5% CO₂. The patch pipettes

were pulled from borosilicate glass capillary with filaments using a flaming micropipette puller (P-97; Sutter Instruments), and had initial resistance 4~8 MΩ when filled with the internal pipette solution. For current-clamp, the pipette solution was containing (in mM): 120 potassium gluconate, 20 KCl, 10 Hepes, 0.3 EGTA, 2 MgCl₂, and 4 Na₂ATP. The pH was adjusted to 7.3 with KOH, and osmolarity was 290~300 mOsm. Membrane voltage was amplified with a Multiclamp 700B amplifier (Molecular Devices). Data were filtered at 2 kHz and digitized at 10 kHz using a data acquisition interface (1440A; Molecular Devices). Liquid junction potential was corrected. The cell capacity transients were canceled by the capacitive cancellation circuitry on the amplifier and series resistance was compensated for (>80%), and linear leak subtraction was subtracted digitally. The pClamp 10 software (Axon Instruments) was used for signal acquisition and analysis. Small-diameter (<25 μm) neurons were chosen for recording in the experiment. The resting membrane potential (RMP) and the action potential (AP) evoked by a series of ramp current stimulation (time: 1 s; current intensity: 100, 200, and 300 pA) were recorded.

Quantification and statistics

All data were expressed as mean ± SEM. For the analysis of GFAP- or IBA-1 immunoreactivity, the images of the dorsal horn were captured, and a numerical value of the intensity was calculated with a computer-assisted imaging analysis system (ImageJ). The intensity of the background was subtracted in each section. For Western blotting, the density of specific bands was measured with ImageJ. All statistical tests were conducted using two-tailed hypothesis testing. Normality of data were assessed using Kolmogorov-Smirnov test. Rank transformation test was used when the data were not normally distributed (mechanical allodynia behavior). For the immunostaining data, Western blotting, and electrophysiological data, if only two groups were applied, Student's *t* test was used. For the quantitative PCR and immunostaining data, if more than three groups were applied, one-way ANOVA was used. If the differences were significant, post hoc Bonferroni's test was applied to compare the difference between every two groups. For the behavioral test, two-way repeated measures (RM) ANOVA was used. If the differences were significant, post hoc Bonferroni's test was applied to compare values at different time points. All statistical analyses were performed using GraphPad Prism 6 (GraphPad Software, Inc.). P < 0.05 (two-tailed) was considered statistically significant.

Online supplemental material

Fig. S1 shows the generation of *Tlr8*^{-/-} mice and the expression of TLR7 in *Tlr8*^{-/-} mice. Fig. S2 shows the expression of neurochemical markers in the spinal cord, DRG, and skin in WT and *Tlr8*^{-/-} mice. Fig. S3 shows the acute itch, basal pain, and acute pain behaviors of WT and *Tlr8*^{-/-} mice. Fig. S4 shows the expression and distribution of TLR8 in human DRG. Fig. S5 shows the effect of miR-21 on ERK and NFκB activation. Table S1 shows the sequences of miR-21 and *Tlr8* siRNA. Table S2 shows the primer sequences for quantitative PCR. Table S3 shows the primer sequences for single-cell RT-PCR. Table S4 shows the sources of antibodies for immunostaining and Western blotting.

Acknowledgments

This study was supported by the National Natural Science Foundation of China (grant nos. NSFC 81571070 to Z.-J. Zhang, 81771197 to Y.-J. Gao, 31671091 to B.-C. Jiang, and 31700899 to D.-L. Cao), the National Science Foundation of Jiangsu Province (grant no. BK20171255 to Y.-J. Gao), and the Qing Lan Project of Jiangsu Province (to Z.-J. Zhang).

The authors declare no competing financial interests.

Author contributions: Z.-J. Zhang performed the immunostaining, behavioral test, and analyzed the data. J.-S. Guo performed quantitative PCR, behavioral tests, Western blotting, and immunostaining. S.-S. Li performed the quantitative PCR, immunostaining, Western blotting, and behavioral test. X.-B. Wu conducted the electrophysiological recording. D.-L. Cao performed the single-cell PCR and participated in the immunostaining experiments. B.-C. Jiang performed *in situ* hybridization experiment. P.-B. Jing performed itch behavioral tests. X.-Q. Bai, C.-H. Li, and Y. Lu participated in the behavioral tests. Z.-H. Wu participated in the quantification of the immunostaining results. Y.-J. Gao coordinated and supervised the project. Y.-J. Gao and Z.-J. Zhang designed the experiments and wrote the manuscript.

Submitted: 30 April 2018

Revised: 10 September 2018

Accepted: 17 October 2018

References

- Akira, S., and K. Takeda. 2004. Toll-like receptor signalling. *Nat. Rev. Immunol.* 4:499–511. <https://doi.org/10.1038/nri1391>
- Akira, S., S. Uematsu, and O. Takeuchi. 2006. Pathogen recognition and innate immunity. *Cell.* 124:783–801. <https://doi.org/10.1016/j.cell.2006.02.015>
- Alexopoulou, L., A.C. Holt, R. Medzhitov, and R.A. Flavell. 2001. Recognition of double-stranded RNA and activation of NF-κappaB by Toll-like receptor 3. *Nature.* 413:732–738. <https://doi.org/10.1038/35099560>
- Barabas, M.E., E.A. Kossyreva, and C.L. Stucky. 2012. TRPA1 is functionally expressed primarily by IB4-binding, non-peptidergic mouse and rat sensory neurons. *PLoS One.* 7:e47988. <https://doi.org/10.1371/journal.pone.0047988>
- Belkouch, M., M.A. Dansereau, A. Réaux-Le Goazigo, J. Van Steenwinckel, N. Beaudet, A. Chraibi, S. Melik-Parsadanian, and P. Sarret. 2011. The chemokine CCL2 increases Nav1.8 sodium channel activity in primary sensory neurons through a Gβγ-dependent mechanism. *J. Neurosci.* 31:18381–18390. <https://doi.org/10.1523/JNEUROSCI.3386-11.2011>
- Bergström, B., M.H. Aune, J.A. Awuh, J.F. Kojen, K.J. Blix, L. Ryan, T.H. Flo, T.E. Mollnes, T. Espenvik, and J. Stenvik. 2015. TLR8 Senses *Staphylococcus aureus* RNA in Human Primary Monocytes and Macrophages and Induces IFN-β Production via a TAK1-IKKβ-IRF5 Signaling Pathway. *J. Immunol.* 195:1100–1111. <https://doi.org/10.4049/jimmunol.1403176>
- Berta, T., C.K. Park, Z.Z. Xu, R.G. Xie, T. Liu, N. Lü, Y.C. Liu, and R.R. Ji. 2014. Extracellular caspase-6 drives murine inflammatory pain via microbial TNF-α secretion. *J. Clin. Invest.* 124:1173–1186. <https://doi.org/10.1172/JCI72230>
- Bsibsi, M., R. Ravid, D. Gveric, and J.M. van Noort. 2002. Broad expression of Toll-like receptors in the human central nervous system. *J. Neuropathol. Exp. Neurol.* 61:1013–1021. <https://doi.org/10.1093/jnen/61.11.1013>
- Cavanaugh, D.J., H. Lee, L. Lo, S.D. Shields, M.J. Zylka, A.I. Basbaum, and D.J. Anderson. 2009. Distinct subsets of unmyelinated primary sensory fibers mediate behavioral responses to noxious thermal and mechanical stimuli. *Proc. Natl. Acad. Sci. USA.* 106:9075–9080. <https://doi.org/10.1073/pnas.0901507106>
- Christianson, C.A., D.S. Dumla, J.A. Stokes, E.A. Dennis, C.I. Svensson, M. Corr, and T.L. Yaksh. 2011. Spinal TLR4 mediates the transition to a persistent mechanical hypersensitivity after the resolution of inflammation in serum-transferred arthritis. *Pain.* 152:2881–2891. <https://doi.org/10.1016/j.pain.2011.09.020>

- Chuang, T.H., and R.J. Ulevitch. 2000. Cloning and characterization of a sub-family of human toll-like receptors: hTLR7, hTLR8 and hTLR9. *Eur. Cytokine Netw.* 11:372–378.
- Crack, P.J., and P.J. Bray. 2007. Toll-like receptors in the brain and their potential roles in neuropathology. *Immunol. Cell Biol.* 85:476–480. <https://doi.org/10.1038/sj.icb.7100103>
- Demaria, O., P.P. Pagni, S. Traub, A. de Gassart, N. Branzk, A.J. Murphy, D.M. Valenzuela, G.D. Yancopoulos, R.A. Flavell, and L. Alexopoulou. 2010. TLR8 deficiency leads to autoimmunity in mice. *J. Clin. Invest.* 120:3651–3662.
- Diebold, S.S., T. Kaisho, H. Hemmi, S. Akira, and C. Reis e Sousa. 2004. Innate antiviral responses by means of TLR7-mediated recognition of single-stranded RNA. *Science.* 303:1529–1531. <https://doi.org/10.1126/science.1093616>
- Dixon, W.J. 1980. Efficient analysis of experimental observations. *Annu. Rev. Pharmacol. Toxicol.* 20:441–462. <https://doi.org/10.1146/annurev.pa.20.040180.000230>
- Fabbri, M., A. Paone, F. Calore, R. Galli, E. Gaudio, R. Santhanam, F. Lovat, P. Fadda, C. Mao, G.J. Nuovo, et al. 2012. MicroRNAs bind to Toll-like receptors to induce prometastatic inflammatory response. *Proc. Natl. Acad. Sci. USA.* 109:E2110–E2116. <https://doi.org/10.1073/pnas.1209414109>
- Gao, Y.J., and R.R. Ji. 2010. Targeting astrocyte signaling for chronic pain. *Neurotherapeutics.* 7:482–493. <https://doi.org/10.1016/j.nurt.2010.05.016>
- Gao, Y.J., L. Zhang, O.A. Samad, M.R. Suter, K. Yasuhiko, Z.Z. Xu, J.Y. Park, A.L. Lind, Q. Ma, and R.R. Ji. 2009. JNK-induced MCP-1 production in spinal cord astrocytes contributes to central sensitization and neuropathic pain. *J. Neurosci.* 29:4096–4108. <https://doi.org/10.1523/JNEUROSCI.3623-08.2009>
- Grace, P.M., K.A. Strand, E.L. Galer, D.J. Urban, X. Wang, M.V. Baratta, T.J. Fabisiak, N.D. Anderson, K. Cheng, L.I. Greene, et al. 2016. Morphine paradoxically prolongs neuropathic pain in rats by amplifying spinal NLRP3 inflammasome activation. *Proc. Natl. Acad. Sci. USA.* 113:E3441–E3450. <https://doi.org/10.1073/pnas.1602070113>
- Hargreaves, K., R. Dubner, F. Brown, C. Flores, and J. Joris. 1988. A new and sensitive method for measuring thermal nociception in cutaneous hyperalgesia. *Pain.* 32:77–88. [https://doi.org/10.1016/0304-3959\(88\)90026-7](https://doi.org/10.1016/0304-3959(88)90026-7)
- Heil, F., H. Hemmi, H. Hochrein, F. Ampenberger, C. Kirschning, S. Akira, G. Lipford, H. Wagner, and S. Bauer. 2004. Species-specific recognition of single-stranded RNA via toll-like receptor 7 and 8. *Science.* 303:1526–1529. <https://doi.org/10.1126/science.1093620>
- Hemmi, H., O. Takeuchi, T. Kawai, T. Kaisho, S. Sato, H. Sanjo, M. Matsumoto, K. Hoshino, H. Wagner, K. Takeda, and S. Akira. 2000. A Toll-like receptor recognizes bacterial DNA. *Nature.* 408:740–745. <https://doi.org/10.1038/35047123>
- Hylden, J.L., and G.L. Wilcox. 1980. Intrathecal morphine in mice: a new technique. *Eur. J. Pharmacol.* 67:313–316. [https://doi.org/10.1016/0014-2999\(80\)90515-4](https://doi.org/10.1016/0014-2999(80)90515-4)
- Ishii, N., K. Funami, M. Tatematsu, T. Seya, and M. Matsumoto. 2014. Endosomal localization of TLR8 confers distinctive proteolytic processing on human myeloid cells. *J. Immunol.* 193:5118–5128. <https://doi.org/10.4049/jimmunol.1401375>
- Itoh, H., M. Tatematsu, A. Watanabe, K. Iwano, K. Funami, T. Seya, and M. Matsumoto. 2011. UNC93B1 physically associates with human TLR8 and regulates TLR8-mediated signaling. *PLoS One.* 6:e28500. <https://doi.org/10.1371/journal.pone.0028500>
- Ji, R.R. 2015. Neuroimmune interactions in itch: Do chronic itch, chronic pain, and chronic cough share similar mechanisms? *Pulm. Pharmacol. Ther.* 35:81–86. <https://doi.org/10.1016/j.pupt.2015.09.001>
- Ji, R.R., R.W. Gereau IV, M. Malcangio, and G.R. Strichartz. 2009. MAP kinase and pain. *Brain Res. Brain Res. Rev.* 60:135–148. <https://doi.org/10.1016/j.brainresrev.2008.12.011>
- Jiang, B.C., D.L. Cao, X. Zhang, Z.J. Zhang, L.N. He, C.H. Li, W.W. Zhang, X.B. Wu, T. Berta, R.R. Ji, and Y.J. Gao. 2016. CXCL13 drives spinal astrocyte activation and neuropathic pain via CXCR5. *J. Clin. Invest.* 126:745–761. <https://doi.org/10.1172/JCI81950>
- Jin, X., and R.W. Gereau IV. 2006. Acute p38-mediated modulation of tetrodotoxin-resistant sodium channels in mouse sensory neurons by tumor necrosis factor-alpha. *J. Neurosci.* 26:246–255. <https://doi.org/10.1523/JNEUROSCI.3858-05.2006>
- Jurk, M., F. Heil, J. Vollmer, C. Schetter, A.M. Krieg, H. Wagner, G. Lipford, and S. Bauer. 2002. Human TLR7 or TLR8 independently confer responsiveness to the antiviral compound R-848. *Nat. Immunol.* 3:499. <https://doi.org/10.1038/ni0602-499>
- Kawai, T., and S. Akira. 2010. The role of pattern-recognition receptors in innate immunity: update on Toll-like receptors. *Nat. Immunol.* 11:373–384. <https://doi.org/10.1038/ni.1863>
- Kawai, T., and S. Akira. 2011. Toll-like receptors and their crosstalk with other innate receptors in infection and immunity. *Immunity.* 34:637–650. <https://doi.org/10.1016/j.immuni.2011.05.006>
- Kawasaki, Y., L. Zhang, J.K. Cheng, and R.R. Ji. 2008. Cytokine mechanisms of central sensitization: distinct and overlapping role of interleukin-1beta, interleukin-6, and tumor necrosis factor-alpha in regulating synaptic and neuronal activity in the superficial spinal cord. *J. Neurosci.* 28:5189–5194. <https://doi.org/10.1523/JNEUROSCI.3338-07.2008>
- Kielian, T. 2006. Toll-like receptors in central nervous system glial inflammation and homeostasis. *J. Neurosci. Res.* 83:711–730. <https://doi.org/10.1002/jnr.20767>
- Kim, D., M.A. Kim, I.H. Cho, M.S. Kim, S. Lee, E.K. Jo, S.Y. Choi, K. Park, J.S. Kim, S. Akira, et al. 2007. A critical role of toll-like receptor 2 in nerve injury-induced spinal cord glial cell activation and pain hypersensitivity. *J. Biol. Chem.* 282:14975–14983. <https://doi.org/10.1074/jbc.M607277200>
- Krüger, A., M. Oldenburg, C. Chebrolu, D. Beisser, J. Kolter, A.M. Sigmund, J. Steinmann, S. Schäfer, H. Hochrein, S. Rahmann, et al. 2015. Human TLR8 senses UR/URR motifs in bacterial and mitochondrial RNA. *EMBO Rep.* 16:1656–1663. <https://doi.org/10.15252/embr.201540861>
- Lee, B.L., J.E. Moon, J.H. Shu, L. Yuan, Z.R. Newman, R. Schekman, and G.M. Barton. 2013. UNC93B1 mediates differential trafficking of endosomal TLRs. *eLife.* 2:e00291. <https://doi.org/10.7554/eLife.00291>
- Lee, J.H., C.K. Park, G. Chen, Q. Han, R.G. Xie, T. Liu, R.R. Ji, and S.Y. Lee. 2014. A monoclonal antibody that targets a NaV1.7 channel voltage sensor for pain and itch relief. *Cell.* 157:1393–1404. <https://doi.org/10.1016/j.cell.2014.03.064>
- Lehmann, S.M., C. Krüger, B. Park, K. Derkow, K. Rosenberger, J. Baumgart, T. Trimbuch, G. Eom, M. Hinz, D. Kaul, et al. 2012. An unconventional role for miRNA: let-7 activates Toll-like receptor 7 and causes neurodegeneration. *Nat. Neurosci.* 15:827–835. <https://doi.org/10.1038/nn.3113>
- Li, S., B. Yu, S. Wang, Y. Gu, D. Yao, Y. Wang, T. Qian, F. Ding, and X. Gu. 2012. Identification and functional analysis of novel micro-RNAs in rat dorsal root ganglia after sciatic nerve resection. *J. Neurosci. Res.* 90:791–801. <https://doi.org/10.1002/jnr.22814>
- Li, Y., P. Adamek, H. Zhang, C.E. Tatsui, L.D. Rhines, P. Mrozko, Q. Li, A.K. Kosturakis, R.M. Cassidy, D.S. Harrison, et al. 2015. The Cancer Chemos therapeutic Paclitaxel Increases Human and Rodent Sensory Neuron Responses to TRPV1 by Activation of TLR4. *J. Neurosci.* 35:13487–13500. <https://doi.org/10.1523/JNEUROSCI.1956-15.2015>
- Liu, T., Z.Z. Xu, C.K. Park, T. Berta, and R.R. Ji. 2010. Toll-like receptor 7 mediates pruritus. *Nat. Neurosci.* 13:1460–1462. <https://doi.org/10.1038/nn.2683>
- Liu, T., T. Berta, Z.Z. Xu, C.K. Park, L. Zhang, N. Lü, Q. Liu, Y. Liu, Y.J. Gao, Y.C. Liu, et al. 2012a. TLR3 deficiency impairs spinal cord synaptic transmission, central sensitization, and pruritus in mice. *J. Clin. Invest.* 122:2195–2207. <https://doi.org/10.1172/JCI45414>
- Liu, T., Y.J. Gao, and R.R. Ji. 2012b. Emerging role of Toll-like receptors in the control of pain and itch. *Neurosci. Bull.* 28:131–144. <https://doi.org/10.1007/s12264-012-1219-5>
- Liu, T., Q. Han, G. Chen, Y. Huang, L.X. Zhao, T. Berta, Y.J. Gao, and R.R. Ji. 2016. Toll-like receptor 4 contributes to chronic itch, allodynia, and spinal astrocyte activation in male mice. *Pain.* 157:806–817. <https://doi.org/10.1097/j.pain.0000000000000439>
- Lu, H., G.N. Dietsch, M.A. Matthews, Y. Yang, S. Ghanekar, M. Inokuma, M. Suni, V.C. Maino, K.E. Henderson, J.J. Howbert, et al. 2012. VTX-2337 is a novel TLR8 agonist that activates NK cells and augments ADCC. *Clin. Cancer Res.* 18:499–509. <https://doi.org/10.1158/1078-0432.CCR-11-1625>
- Ma, Y., J. Li, I. Chiu, Y. Wang, J.A. Sloane, J. Lü, B. Kosaras, R.L. Sidman, J.J. Volpe, and T. Vartanian. 2006. Toll-like receptor 8 functions as a negative regulator of neurite outgrowth and inducer of neuronal apoptosis. *J. Cell Biol.* 175:209–215. <https://doi.org/10.1083/jcb.200606016>
- Ma, Y., R.L. Haynes, R.L. Sidman, and T. Vartanian. 2007. TLR8: an innate immune receptor in brain, neurons and axons. *Cell Cycle.* 6:2859–2868. <https://doi.org/10.4161/cc.6.23.5018>
- Martinez, J., X. Huang, and Y. Yang. 2010. Toll-like receptor 8-mediated activation of murine plasmacytoid dendritic cells by vaccinia viral DNA. *Proc. Natl. Acad. Sci. USA.* 107:6442–6447. <https://doi.org/10.1073/pnas.0913291107>
- Obata, K., H. Yamanaka, Y. Dai, T. Mizushima, T. Fukuoka, A. Tokunaga, and K. Noguchi. 2004a. Differential activation of MAPK in injured and uninjured DRG neurons following chronic constriction injury of the sci-

- atic nerve in rats. *Eur. J. Neurosci.* 20:2881–2895. <https://doi.org/10.1111/j.1460-9568.2004.03754.x>
- Obata, K., H. Yamanaka, K. Kobayashi, Y. Dai, T. Mizushima, H. Katsura, T. Fukuoka, A. Tokunaga, and K. Noguchi. 2004b. Role of mitogen-activated protein kinase activation in injured and intact primary afferent neurons for mechanical and heat hypersensitivity after spinal nerve ligation. *J. Neurosci.* 24:10211–10222. <https://doi.org/10.1523/JNEUROSCI.3388-04.2004>
- Olson, J.K., and S.D. Miller. 2004. Microglia initiate central nervous system innate and adaptive immune responses through multiple TLRs. *J. Immunol.* 173:3916–3924. <https://doi.org/10.4049/jimmunol.173.6.3916>
- Park, C.K., Z.Z. Xu, T. Berta, Q. Han, G. Chen, X.J. Liu, and R.R. Ji. 2014. Extracellular microRNAs activate nociceptor neurons to elicit pain via TLR and TRPA1. *Neuron.* 82:47–54. <https://doi.org/10.1016/j.neuron.2014.02.011>
- Prinz, M., F. Garbe, H. Schmidt, A. Mildner, I. Gutcher, K. Wolter, M. Piesche, R. Schroers, E. Weiss, C.J. Kirschning, et al. 2006. Innate immunity mediated by TLR9 modulates pathogenicity in an animal model of multiple sclerosis. *J. Clin. Invest.* 116:456–464. <https://doi.org/10.1172/JCI26078>
- Qi, J., K. Buzas, H. Fan, J.I. Cohen, K. Wang, E. Mont, D. Klinman, J.J. Oppenheim, and O.M. Howard. 2011. Painful pathways induced by TLR stimulation of dorsal root ganglion neurons. *J. Immunol.* 186:6417–6426. <https://doi.org/10.4049/jimmunol.1001241>
- Sakai, A., and H. Suzuki. 2013. Nerve injury-induced upregulation of miR-21 in the primary sensory neurons contributes to neuropathic pain in rats. *Biochem. Biophys. Res. Commun.* 435:176–181. <https://doi.org/10.1016/j.bbrc.2013.04.089>
- Sakai, A., F. Saitow, N. Miyake, K. Miyake, T. Shimada, and H. Suzuki. 2013. miR-7a alleviates the maintenance of neuropathic pain through regulation of neuronal excitability. *Brain.* 136:2738–2750. <https://doi.org/10.1093/brain/awt191>
- Santa-Cecília, F.V., D.W. Ferreira, R.M. Guimaraes, N.T. Cecilio, M.M. Fonseca, A.H. Lopes, M. Davoli-Ferreira, R. Kusuda, G.R. Souza, U. Nachbur, et al. 2018. The NOD2 signaling in peripheral macrophages contributes to neuropathic pain development. *Pain.* In press. <https://doi.org/10.1097/j.pain.0000000000001383>
- Sarvestani, S.T., B.R. Williams, and M.P. Gantier. 2012. Human Toll-like receptor 8 can be cool too: implications for foreign RNA sensing. *J. Interferon Cytokine Res.* 32:350–361. <https://doi.org/10.1089/jir.2012.0014>
- Song, X.J., J.H. Zheng, J.L. Cao, W.T. Liu, X.S. Song, and Z.J. Huang. 2008. EphrinB-EphB receptor signaling contributes to neuropathic pain by regulating neural excitability and spinal synaptic plasticity in rats. *Pain.* 139:168–180. <https://doi.org/10.1016/j.pain.2008.03.019>
- Stamboulian, S., J.S. Choi, H.S. Ahn, Y.W. Chang, L. Tyrrell, J.A. Black, S.G. Waxman, and S.D. Dib-Hajj. 2010. ERK1/2 mitogen-activated protein kinase phosphorylates sodium channel Na(v)1.7 and alters its gating properties. *J. Neurosci.* 30:1637–1647. <https://doi.org/10.1523/JNEUROSCI.4872-09.2010>
- Stemkowski, P.L., and P.A. Smith. 2012. Long-term IL-1 β exposure causes subpopulation-dependent alterations in rat dorsal root ganglion neuron excitability. *J. Neurophysiol.* 107:1586–1597. <https://doi.org/10.1152/jn.00587.2011>
- Strickland, I.T., L. Richards, F.E. Holmes, D. Wynick, J.B. Uney, and L.F. Wong. 2011. Axotomy-induced miR-21 promotes axon growth in adult dorsal root ganglion neurons. *PLoS One.* 6:e23423. <https://doi.org/10.1371/journal.pone.0023423>
- Tanga, F.Y., N. Nutile-McMenemy, and J.A. DeLeo. 2005. The CNS role of Toll-like receptor 4 in innate neuroimmunity and painful neuropathy. *Proc. Natl. Acad. Sci. USA.* 102:5856–5861. <https://doi.org/10.1073/pnas.0501634102>
- Tanji, H., U. Ohto, T. Shibata, K. Miyake, and T. Shimizu. 2013. Structural reorganization of the Toll-like receptor 8 dimer induced by agonistic ligands. *Science.* 339:1426–1429. <https://doi.org/10.1126/science.1229159>
- Wu, F.X., J.J. Bian, X.R. Miao, S.D. Huang, X.W. Xu, D.J. Gong, Y.M. Sun, Z.J. Lu, and W.F. Yu. 2010. Intrathecal siRNA against Toll-like receptor 4 reduces nociception in a rat model of neuropathic pain. *Int. J. Med. Sci.* 7:251–259. <https://doi.org/10.7150/ijms.7.251>
- Wu, X.B., D.L. Cao, X. Zhang, B.C. Jiang, L.X. Zhao, B. Qian, and Y.J. Gao. 2016. CXCL13/CXCR5 enhances sodium channel Nav1.8 current density via p38 MAP kinase in primary sensory neurons following inflammatory pain. *Sci. Rep.* 6:34836. <https://doi.org/10.1038/srep34836>
- Xie, R.G., Y.J. Gao, C.K. Park, N. Lu, C. Luo, W.T. Wang, S.X. Wu, and R.R. Ji. 2018. Spinal CCL2 Promotes Central Sensitization, Long-Term Potentiation, and Inflammatory Pain via CCR2: Further Insights into Molecular, Synaptic, and Cellular Mechanisms. *Neurosci. Bull.* 34:13–21. <https://doi.org/10.1007/s12264-017-0106-5>
- Xu, J.T., W.J. Xin, Y. Zang, C.Y. Wu, and X.G. Liu. 2006. The role of tumor necrosis factor-alpha in the neuropathic pain induced by Lumbar 5 ventral root transection in rat. *Pain.* 123:306–321. <https://doi.org/10.1016/j.pain.2006.03.011>
- Zhang, J.M., D.F. Donnelly, X.J. Song, and R.H. Lamotte. 1997. Axotomy increases the excitability of dorsal root ganglion cells with unmyelinated axons. *J. Neurophysiol.* 78:2790–2794. <https://doi.org/10.1152/jn.1997.78.5.2790>
- Zhang, Q., D.L. Cao, Z.J. Zhang, B.C. Jiang, and Y.J. Gao. 2016. Chemokine CXCL13 mediates orofacial neuropathic pain via CXCR5/ERK pathway in the trigeminal ganglion of mice. *J. Neuroinflammation.* 13:183. <https://doi.org/10.1186/s12974-016-0652-1>
- Zhang, Z.J., D.L. Cao, X. Zhang, R.R. Ji, and Y.J. Gao. 2013. Chemokine contribution to neuropathic pain: respective induction of CXCL1 and CXCR2 in spinal cord astrocytes and neurons. *Pain.* 154:2185–2197. <https://doi.org/10.1016/j.pain.2013.07.002>
- Zylka, M.J., F.L. Rice, and D.J. Anderson. 2005. Topographically distinct epidermal nociceptive circuits revealed by axonal tracers targeted to Mrgpr. *Neuron.* 45:17–25. <https://doi.org/10.1016/j.neuron.2004.12.015>